Astrophysical S factor of the $^{12}C(\alpha,\gamma)^{16}O$ reaction calculated with reduced R-matrix theory

Zhen-Dong An,[1,2] Zhen-Peng Chen,[3,*] Yu-Gang Ma,[1,4,†] Jian-Kai Yu,[5] Ye-Ying Sun,[6] Gong-Tao Fan,[1] Yong-Jiang Li,[1] Hang-Hua Xu,[1,2] Bo-Song Huang,[1,2] and Kan Wang[5]

[1]*Shanghai Institute of Applied Physics, Chinese Academy of Sciences, Shanghai 201800, China*
[2]*University of Chinese Academy of Sciences, Beijing 100049, China*
[3]*Department of Physics, Tsinghua University, Beijing 100084, China*
[4]*ShanghaiTech University, Shanghai 200031, China*
[5]*Department of Engineering Physics, Tsinghua University, Beijing 100084, China*
[6]*Department of Materials, Tsinghua University, Beijing 100084, China*

(Received 2 February 2015; revised manuscript received 2 June 2015; published 6 October 2015)

Determination of the accurate astrophysical S factor of $^{12}C(\alpha,\gamma)^{16}O$ reaction has been regarded as the holy grail of nuclear astrophysics for decades. In current stellar models, a knowledge of that value to better than 10% is desirable. Due to the practical issues, tremendous experimental and theoretical efforts over nearly 50 years are not able to reach this goal, and the published values contradicted with each other strongly and their uncertainties are two times larger than the required precision. To this end we have developed a reduced R-matrix theory based on the classical R-matrix theory of Lane and Thomas, which treats primary transitions to the ground state and four bound states as the independent reaction channels in the channel spin representation. With the coordination of covariance statistics and error-propagation theory, a global fitting for almost all available experimental data of ^{16}O system has been multi-iteratively analyzed by our powerful code. A reliable, accurate, and self-consistent astrophysical S factor of $^{12}C(\alpha,\gamma)^{16}O$ was obtained with a recommended value $S_{tot}(0.3\,\text{MeV}) = 162.7 \pm 7.3$ keV b (4.5%) which could meet the required precision.

DOI: 10.1103/PhysRevC.92.045802 PACS number(s): 25.55.−e, 25.40.Lw, 26.20.Fj, 21.10.−k

I. INTRODUCTION

During core He burning, 3α and $^{12}C(\alpha,\gamma)^{16}O$ reactions compete to determine the helium burning timescale, together with the convection mechanism, and the relative abundances of oxygen and carbon prior to core C burning. William A. Fowler, a Nobel laureate in physics in 1983, definitely held a view that the abundance ratio of ^{12}C to ^{16}O and the solar neutrino problem are serious difficulties in the most basic concepts of nuclear astrophysics [1]. The work of many investigators has resulted in a knowledge of the predicted reaction rate of the 3α process within about 10% [2] accuracy at the usual helium-burning temperatures. Unfortunately, the same for the $^{12}C(\alpha,\gamma)^{16}O$ reaction is much-less-well determined, and it is highly desirable to know this rate with an accuracy comparable [3] to that of the 3α process in order to provide adequate constraints on stellar evolution and the synthesis of elements, e.g., the yield of the neutrino-process isotopes ^{7}Li, ^{11}B, ^{19}F, ^{138}La, and ^{180}Ta in core-collapse supernovae [4,5], and the production of the important radioactive nuclei ^{26}Al, ^{44}Ti, and ^{60}Fe [6].

The most direct and trustworthy way to obtain the astrophysical S factor of the $^{12}C(\alpha,\gamma)^{16}O$ reaction is to measure the cross section for that reaction to as low an energy as possible and to extrapolate to energies of astrophysical interest. The astrophysical S factor for the $^{12}C(\alpha,\gamma)^{16}O$ reaction reaction is given by

$$S(E) = \sigma(E)E\exp(2\pi\eta), \tag{1}$$

where $\eta = Z_\alpha Z_C e^2/\hbar v$ is the Sommerfeld parameter for the interaction particles. To investigate the specific role of the ^{16}O nucleus for the S factor, a wealth of experimental data have been accumulated over the past few decades, including the precise measurements of the total cross section of $^{12}C(\alpha,\gamma)^{16}O$ [7–10], γ-ray angular distributions of ground-state transitions [11–22], cascade transitions [8,12,23,24], β-delayed α spectra for ^{16}N [25–28], transfer reactions [29–31], elastic scattering $^{12}C(\alpha,\alpha)^{12}C$ [32–36], and additional particle-reaction pathways $^{12}C(\alpha,\alpha_1)^{12}C$ [37,38] and $^{12}C(\alpha,p)^{15}N$ [37,39] at high energies. However, the complexity of the reaction mechanisms of $^{12}C+\alpha$ makes it extremely difficult to determine the S factor; despite five decades of experimental investigations, the desired accuracy and precision associated with the $^{12}C(\alpha,\gamma)^{16}O$ reaction continues to be an obstacle (see Table I). Two recent collaborations [45,46] and our team [47] have pursued complementary approaches to obtain the inverse $^{16}O(\gamma,\alpha)^{12}C$ reaction to energies lower than the currently achieved, which could offer significant advantages over traditional approaches. But the expected outputs of these proposals in low energy are far from what is required in the stellar models. R-matrix analysis is the most effective method for the fitting and extrapolation of existing data of ^{16}O system, which are main content of this work.

The classical R-matrix theory of Lane and Thomas [48] is deduced the standard R-matrix formulas to describe two-body nuclear reactions. However, these formulas were believed to not be justified for γ radiative capture because of the possibilities of particle production and annihilation, and it is hard to select a suitable channel radius for long-range electromagnetic transition. After that, another paper of Lane [49] expanded the collision matrix to radiative

*zhpchen@tsinghua.edu.cn
†ygma@sinap.ac.cn

TABLE I. Comparison of the astrophysical S factor (keV b) at 0.3 MeV obtained from various fits, including this work, for the $E10$, $E20$, and cascade-transition components, as well as the total.

Reference	$S_{\rm tot}$	S_{E10}	S_{E20}	$S_{\rm cas}$
This work	162.7 ± 7.3	98.0 ± 7.0	56.0 ± 4.1	8.7 ± 1.8
Schürmann [40]	161 ± 19	83.4	73.4	4.4
Oulebsir [31]	175 ± 63	100 ± 28	50 ± 19	
Sayre [41]			62^{+9}_{-6}	
Tang [26]		84 ± 21		
Matei [42]				$S_{6.92} = 7.0 \pm 1.6$
Matei [24]				$S_{6.05} = 25^{+25}_{-16}$
Hammer [43]	162 ± 39	77 ± 17	80 ± 20	4 ± 4
Tischhauser [33]	149 ± 29	80 ± 20	53^{+13}_{-18}	16 ± 16
Kunz [15]	165 ± 50	76 ± 20	85 ± 30	4 ± 4
Brune [29]	159	101 ± 17	42^{+16}_{-23}	16
Ouellet [13]	120 ± 40	79 ± 16	36 ± 6	
Buchmann [44]	165 ± 75	79 ± 21	70 ± 70	16 ± 16

capture for a sum of three parts, viz. an internal resonant, an external resonant and a nonresonant part corresponding to the channel integral from hard-sphere scattering. Based on this conclusion, the angle-integrated cross-section formulas are derived from perturbation theory in Refs. [50,51], and the adjustable parameter of photon reduced-width amplitude can be split into internal and asymptotic channel contributions in practical applications [40,50]. Recently, a vital progress in R-matrix code, AZURE was presented in Refs. [52,53], and it allows simultaneous analysis of the integrated and differential data for the electromagnetic transition.

In the most widely used theory [50], since the S factors of the $E1$ and $E2$ multipoles have different energy dependencies, one must have independent and precise information on each multipole cross section for an extrapolation to 0.3 MeV. So the secondary data of $E1$ and $E2$ multipoles were generally used for the R-matrix analysis in the previous publications. The primary data most often consist of angular distributions measured at many discrete energies. Each primary distribution was then analyzed independently in terms of the appropriate set of Legendre polynomials [11], a non-R-matrix analysis neglecting the energy and angle dependence, to yield the secondary data, σ_{E10} and $\sigma_{E10}/\sigma_{E20}$ at this discrete energy. And these data and their error values, being derived quantities, are no longer proportional to the experimentally measured quantities, i.e., the angular distribution yields, and thus lead to complications and discrepancy for the extrapolation of the $^{12}\mathrm{C}(\alpha,\gamma)\,^{16}\mathrm{O}$ S factor [44].

An R-matrix code for a nuclear system is in principle an exact model as long as a complete set of quantum states of a nuclear system and all the corresponding experimental data can be accurately and simultaneously described (called global fitting). Any inconformity that does not meet the principle will induce inestimable uncertainty, because each channel, each level, and each datum are intimately correlated due to strong interference in the nuclear system. By now, the R-matrix approach mentioned above [50] has become a popular application with the procedure, but their results have very large differences (see Table I). And no one has yet used it to do a global fitting for the $^{16}\mathrm{O}$ system in the astrophysical energy. For these reasons, based on the theory of Lane and Thomas [48], we develop a reduced R-matrix theory to make the global fitting for the special problem of searching for the S factor of $^{12}\mathrm{C}(\alpha,\gamma)\,^{16}\mathrm{O}$.

Section II summarizes the construction of the reduced R-matrix theory and general aspects of the R-matrix approach in the global analysis. Section III presents the construction of reaction channel, evaluation, and fits to experimental data. Results and discussion of the global analysis for each reaction channel are presented in Sec. IV. Finally, conclusions are given in Sec. VII.

II. REDUCED R-MATRIX THEORY

A. The representations for decay channel $\gamma_n + {}^{16}\mathrm{O}_n$

For the $^{12}\mathrm{C}(\alpha,\gamma)\,^{16}\mathrm{O}$ reaction, the decay channel of $\gamma_n + {}^{16}\mathrm{O}_n$ ($n = 0,1,2,3,4$) has the same total angular momentum and parity $\mathbf{J}^\pi$ as the entrance channel $^{12}\mathrm{C}+\alpha$. Three angular momenta are involved at this stage for the state of the compound nucleus, the spins of the target (or residual nucleus) and of the incident (or emitting) particle, and the orbital angular momentum of the incident (or emitting) particle. There are two conventional ways of combining these for the decay channel $\gamma_n + {}^{16}\mathrm{O}_n$. One is the channel spin scheme in which the vector sum of the spins of photon ($\mathbf{I}_\gamma = \mathbf{1}$) and residual nucleus $^{16}\mathrm{O}_n$ ($\mathbf{J_f}$) is first formed giving the channel spin $\mathbf{s}$

$$\mathbf{I}_\gamma + \mathbf{J_f} = \mathbf{s}. \tag{2}$$

Channel spin $\mathbf{s}$ and the orbital angular momentum $\mathbf{l}$ of the photon are then combined to form the spin of the compound nucleus $^{16}\mathrm{O}$,

$$\mathbf{s} + \mathbf{l} = \mathbf{J_i}. \tag{3}$$

Finally, a state in the representation is labeled by the set of quantities $\{\alpha(\mathbf{I}_\gamma\mathbf{J_f})\mathbf{s}/\mathbf{J_i}\mathbf{M}\}$.

The alternative coupling scheme is called by Devons and Goldfarb the "$\mathcal{L}$ representation" [54], which is used widely in the R-matrix theory mentioned above [50,52]. Here, the spin of the photon is combined with the corresponding orbital angular momentum to form the total angular momentum for

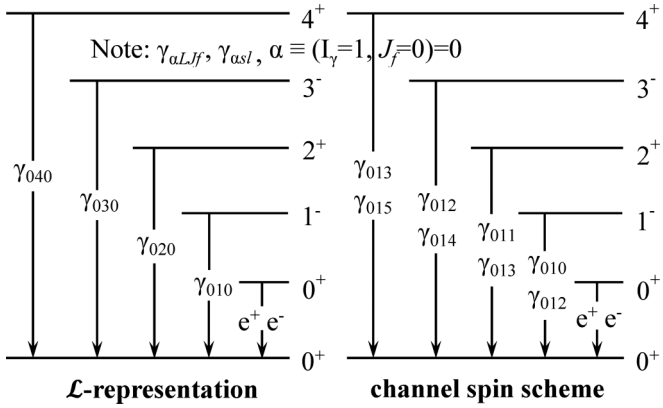

FIG. 1. The electric multipole transition processes to ground state (0^+) described by channel spin scheme and $\mathcal{L}$ representation for ^{16}O system.

the photon states. It gives

$$\mathbf{I}_\gamma + \mathbf{l} = \mathbf{L}. \tag{4}$$

The compound state's spin is then given by

$$\mathbf{L} + \mathbf{J_f} = \mathbf{J_i}. \tag{5}$$

And a state of the compound nucleus is labeled by the set of quantities $\{\alpha(\mathbf{I}_\gamma \mathbf{J_f})\mathbf{L J_f J_i M}\}$ in the scheme.

These two coupling schemes represent the same physical situation in two different representations. In the $\mathcal{L}$ representation, parity conservation implies that

$$\pi_i = \pi_f \pi_\gamma (-1)^{L+P}, \tag{6}$$

with L being the multipolarity and the P being the mode (1 = electric, 0 = magnetic) of the gamma ray, and π_i, π_f, π_γ are the parity of the initial state $\mathbf{J_i}$, final state $\mathbf{J_f}$, and the intrinsic parity of the photon, respectively. Electric multipoles correspond to parity $(-1)^L$ and $l = L \pm 1$, while magnetic multipoles correspond to parity $(-1)^{L+1}$and $l = L$ [54,55]. Based on the expression of (6), we can deduce the parity conservation in the channel spin scheme:

$$\pi_i = \pi_f \pi_\gamma \pi_l = \begin{cases} \pi_f \pi_\gamma (-1)^l, & l = L \pm 1 \\ \pi_f \pi_\gamma (-1)^l, & l = L, \end{cases} \tag{7}$$

where π_l is the parity of the orbital angular momentum for the exit channels.

To comparison the two coupling schemes, Fig. 1 displays the all possible transition processes to the ground state ($J^\pi = 0^+$) of ^{16}O system. The ground-state transition of the $\mathcal{L}$-representation set of components has one value for each decay, which is less than the two components in the channel spin scheme of Fig. 1, and the relevant photon reduced-width amplitude of this processes only exists one parameter in the collision matrix. Only when the channel capture is considered in the $\mathcal{L}$ representation can this parameter be split into internal- and asymptotic-channel contributions [50,52]. So the channel spin scheme provides more subsets to denote the ground-state transition and cascade transition, which is extremely beneficial for a more reliable interpretation of the observed experimental data.

B. Wave function of compound nucleus ^{16}O

For the $^{12}C(\alpha,\gamma)^{16}O$ reaction, the transition of the compound nucleus ^{16}O, the initial radioactive decay to the ground state and the four bound states are regarded as two-body particle-reaction channels, denoted by $\gamma_n + {}^{16}O_n$ ($n = 0,1,2,3,4$), and the reduced masses of these channels are represented by their relativistic energy. It is not necessary to consider how to decay to the ground state finally, so the problem of "particles are created or destroyed" is avoided. The sum of the integrated cross sections of each reaction channel $\gamma_n + {}^{16}O_n$ is equal to the cross section of ^{16}O production.

Owing to the advantage of the channel spin scheme, all the channels of the ^{16}O system are represented as $c = \alpha s l$, where s is the channel spin, l is the relative angular momentum of the interacting particle of entrance or exit channels, and α identifies the interacting particle pair. The primary wave function Ψ can be unfolded with different exit channels ψ_c. Furthermore, ψ_c can be expended with level wave functions X_λ, which have different total angular momentum, parity J^π, and E_λ. Finally, Ψ is expressed by Eq. 2.6 (page 283) in Ref. [48]:

$$\Psi = \sum_c \left[\sum_\lambda \frac{X_\lambda \gamma_{\lambda c}}{E_\lambda - E} \right] D_c^0. \tag{8}$$

So the total wave function for the initial state of ^{16}O can be expanded by the complete orthogonal set, the coefficients of the expanded formula represent the probability of different reaction channels of all sorts of resonance-energy states. Equation (8) demonstrates that, if the primary gamma decay $\gamma_n + {}^{16}O_n$ as the independent two-body reaction channel, the set of level wave functions X_λ of the theoretical model contains all types of γ transitions, whether direct decay to the ground-state transition or to the cascade transition. By using Eq. (8), one can obtain the fundamental R-matrix relationship, the collision matrix, the cross sections, and so on.

For the channel $\gamma_n + {}^{16}O_n$, the electromagnetic interaction is long range, therefore contributions to the collision matrix for radiative capture reactions can come from large distances. Thus, in addition to the internal contribution to the collision matrix, there should also be channel contributions [50]. However, for the chief ground-state transition, owing to the large binding energy (7.16 MeV) of the ^{16}O with respect to the $\alpha + {}^{12}C$ threshold, its wave function decreases rapidly when the radius is larger than a certain value. So the internal contribution is strongly dominant, and the external part can be neglected. The results in Refs. [23,50] prove to be reasonable and effective for this approximation, that the external contribution accounts for less than 3% at 0.3 MeV. For the cascade transitions, a parameter for the final state can be used to characterize the direct capture process of these transitions (see the parameters table). So a global fitting for the whole ^{16}O system can be done by using the standard R-matrix formulas of Ref. [48] with a suitable channel radius.

C. Mathematical formalism of random access code

The practical formulas of our R-matrix Analyzing Code (RAC code) are introduced from the literature [57–59]. On the R-matrix and the reaction cross sections, the code is

strictly compiled in accordance with the formulas of the classic literature [48], without any approximation.

Explicitly, the R matrix, which represents all the internal information concerning the structure of the compound system, is defined as

$$\mathbf{R}^{J}_{\alpha' s' l', \alpha s l} = \sum_{\lambda\mu}^{N} \gamma^{J}_{\alpha' s' l'} \gamma^{J}_{\alpha s l} A_{\lambda\mu} \delta_{J J_0}, \tag{9}$$

where $\gamma^{J}_{\alpha' s' l'}$ and $\gamma^{J}_{\alpha s l}$ are the reduced-width amplitude of the entrance and exit channels, respectively. The matrix $\mathbf{A}_{\lambda\mu}$ is defined by its inverse

$$[A^{-1}]_{\lambda\mu} = (E_\lambda - E)\delta_{\lambda\mu} - \Delta_{\lambda\mu} - \frac{i\Gamma_{\lambda\mu}}{2}, \tag{10}$$

where E_λ is the position of the resonance level, $\Delta_{\lambda\mu}$ is the energy shift, and $\Gamma_{\lambda\mu}$ is the total reduced channel width, which can represent the contribution of all nonconsidered channels, such as the $^{12}\mathrm{C}(\alpha,\alpha_2)\,^{12}\mathrm{C}$ in our fit. The additional quantity appearing in Eq. (10) is

$$\Delta_{\lambda\mu} = -\sum_{\alpha s l}^{N} (S_{\lambda\mu} - B_{\lambda\mu}) \gamma_{\alpha' s' l'} \gamma_{\alpha s l}, \tag{11}$$

where $S_{\lambda\mu}$ is the shift factor calculated at the channel radius, and $B_{\lambda\mu}$ is a constant boundary parameter.

The literature of Lane and Thomas (page 273) [48], gives the correction formula for the level width $\Gamma_{\lambda c}$ and level shift $\Delta_{\lambda c}$:

$$\Gamma_{\lambda c} = 2P_c \gamma^2_{\lambda c} / d_c, \tag{12}$$

$$\Delta_{\lambda c} = \frac{P_c\left(R^0_{cc} P_c\right) - S^0_c\left(1 - R^0_{cc} S^0_c\right)}{d_c} \gamma^2_{\lambda c}, \tag{13}$$

where

$$d_c = \left(1 - R^0_{cc} S^0_c\right)^2 + \left(R^0_{cc} P_c\right)^2. \tag{14}$$

Here, λ is the level of the c reaction channel, P_c is the penetration factor, and the notation zero indicates the constant background. These formulas are workable only based on an approximation of a single level. The RAC is the multichannel and multilevel R-matrix formula without a constant background. When calculating the width and shift of some levels, the calculated values of the R-matrix with the remaining levels are taken as the constant background of the level. The observed width can be related to the physical reduced width amplitudes with the following formula:

$$\Gamma^{\mathrm{obs}}_{\lambda c} = \Gamma_{\lambda c} \left(1 + \sum_k \gamma^2_{\lambda k} \frac{dS_k}{dE}\right)^{-1}_{E_\lambda}. \tag{15}$$

The total width for a state λ is then the sum

$$\Gamma^{\mathrm{obs}}_{\lambda} = \sum_c \Gamma^{\mathrm{obs}}_{\lambda c}. \tag{16}$$

With the relation between the T matrix and the U matrix from

$$T^{J}_{\alpha' s' l', a s l} = e^{2i\omega_{al}} \delta_{\alpha' s' l', \alpha s l} - U^{J}_{\alpha' s' l', \alpha s l}, \tag{17}$$

for a reaction going through $\alpha' \to \alpha$, the angle-integrated cross section is

$$\sigma_{\alpha', a} = \frac{\pi}{k^2_\alpha} \sum_{s l' s' l J} \frac{(2J+1)}{(2I_1+1)(2I_2+1)} \left|T^{J}_{\alpha' s' l', a s l}\right|^2, \tag{18}$$

and I_1 and I_2 are the projectile and target spins, respectively. Note that the above equation does not hold for charged-particle elastic scattering.

For the corresponding differential-cross-section formula, a more rigorous calculation is involved in Ref. [48]:

$$\frac{d\sigma_{\alpha,\alpha'}}{d\Omega_{\alpha'}} = \frac{1}{(2I_1+1)(2I_2+1)} \sum_{s s' \nu \nu'} |A_{\alpha' s' \nu', \alpha s \nu}(\Omega_{\alpha'})|^2, \tag{19}$$

where $A_{\alpha' s' \nu', \alpha s \nu}$ are the amplitudes of the outgoing waves.

$$A_{\alpha' s' \nu', \alpha s \nu}(\Omega_{\alpha'}) = \frac{\sqrt{\pi}}{k_\alpha} \Bigg[- C_{\alpha'}(\theta_{\alpha'}) \delta_{\alpha' s' \nu', \alpha s \nu} + i \sum_{J M l l' m'} \sqrt{2l+1} (s l \nu 0 | J M)(s' l' \nu' m' | J M) \times T^{J}_{\alpha' s' l', \alpha s l} Y^{(l')}_{m'}(\Omega_{\alpha'}) \Bigg]. \tag{20}$$

Several new quantities have been introduced in Eq. (20) to define the angular dependence of the cross section. The term $-C_{\alpha'}(\theta_{\alpha'})$ represents the Coulomb amplitudes, while $Y^{(l')}_{m'}$ is the spherical harmonics function.

The transverse character of electromagnetic waves requires that the projections of intrinsic spins of photon cannot be zero. For the transition with $\mathbf{J}_f = 0$, when $\nu' = 0$, the γ-spin projection is zero. So when using Eq. (19) to calculate the angular distribution of γ decay, as long as we ignore the loop for $\nu' = 0$, the calculation will not include the contribution of the γ-spin-projection component of zero. When this method is adopted, the angle-integrated cross section can be described effectively in our fit, but the corresponding differential cross section is not accurately fit. So in the actual work, the longitudinal contribution of the photon is employed to give a precise description for the all available data.

D. Covariance statistic and error-propagation law

The uncertainty determination of the extrapolated S factor requires an error propagation of all relevant fit parameters through the fit function, taking into account the covariances. The theoretical formula for error propagation [56] for our R-matrix-model fitting is

$$\mathbf{y} - \mathbf{y}_0 = \mathbf{D}(\mathbf{P} - \mathbf{P}_0), \tag{21}$$

$$D_{ki} = (\partial y_k / \partial P_i)_0. \tag{22}$$

Here $\mathbf{y}$ refers to vector of calculated values, $\mathbf{D}$ to the sensitivity matrix, $\mathbf{P}$ to the vector of R-matrix parameters. The subscript 0 means the optimized original value, k and i stand for fitted data and the R-matrix parameter, respectively. The covariance matrix of the parameter $\mathbf{P}$ is

$$\mathbf{V_P} = (\mathbf{D}^{+}\mathbf{V}^{-1}\mathbf{D})^{-1}. \tag{23}$$

Here $\mathbf{V}$ refers to covariance matrix of the data to be fit, and its inversion matrix can be expressed as

$$\mathbf{V}^{-1} = \begin{pmatrix} \mathbf{V_1^{-1}} & & & 0 \\ & \mathbf{V_2^{-1}} & & \\ & & \ddots & \\ 0 & & & \mathbf{V_k^{-1}} \end{pmatrix}, \quad (24)$$

where $\mathbf{V}_1, \mathbf{V}_2, \ldots, \mathbf{V}_k$ refer to the covariance matrices of the subset data, which are independent of each other. The covariance matrix of calculated values is

$$\mathbf{V_y} = \mathbf{D V_P D}^{+}. \quad (25)$$

The sensitivity matrix is quite useful in eliminating redundant fit parameters and in understanding which fit parameters are the most effective on the low-energy extrapolation of the S factor, as discussed below.

The formula adopted for optimizing with R-matrix fitting is

$$\chi^2 = (\eta - \mathbf{y})^{+} \mathbf{V}^{-1} (\eta - \mathbf{y}) \Rightarrow \text{minimum}. \quad (26)$$

Here, η refers to the vector of experimental data, $\mathbf{y}$ refers to the vector of calculated values. By using covariance statistics and the error propagation law, we can get accurate expected values and a standard deviation of the S factor.

In addition, the Peelle pertinent puzzle (PPP) was corrected by the method used in Ref. [59]. The RAC was used to produce accurate (error = 1%) ^{6}Li(n,α) and ^{10}B(n,α) cross sections for the International Evaluation of Neutron Cross Section Standards [58,59]. And the RAC was comprehensively compared with the R-matrix code EDA and SAMMY from the USA [58,59]: the results were closely identical when the same parameters were used. To verify the performance of the R-matrix code for the ^{16}N α spectrum, we repeated the analysis of Ref. [26] using their input data, and the same results were obtained. In a word, it is proven that the RAC code is reliable.

III. EVALUATION AND FIT TO EXPERIMENTAL DATA

A. Construction of reaction channel

The observed position, width or lifetime of ^{16}O levels are displayed in Fig. 2 up to the 17.5-MeV-energy region from Ref. [60]. The cascade-transition data in Refs. [8,42] reveal several γ-ray cascade transitions from the 1^-, 3^-, and 2^+ states at $E_x = 7.12$, 11.49, and 11.51 MeV, respectively, which are considered in our fit. Except the level $J^\pi = 2^-$ ($E_x = 8.872$ MeV), the other 31 levels contain the $\alpha + {}^{12}$C reaction channel. Based on the level scheme of the ^{16}O nucleus, the R-matrix analysis of the ^{16}O compound nucleus considers the one particle entrance channel ^{12}C $+\alpha$, and the eight particle exit channels as shown in Table II. The R-matrix calculations were performed for $J^\pi = 0^+$ (four real levels, one background level), $J^\pi = 1^-$ (five real levels, one background level), $J^\pi = 2^+$ and 3^- (seven real levels, and one background level), $J^\pi = 4^+$ (four real levels, one background level), $J^\pi = 5^-$ (two levels, one background level), and $J^\pi = 6^+$ (two real levels). The available data sets cover the energy from $E_{\text{c.m.}} = 0.9$ MeV to $E_{\text{c.m.}} = 7.5$ MeV in this fit, so the parameters above this region are fixed at values determined from Ref. [60].

TABLE II. The reaction channels in our fit including Q values, radii, the maximum of the orbital angular momentum, and the data, respectively, in the R-matrix calculation. For the capture reaction, magnetic L-pole radiation is significantly weaker than the corresponding electric L-pole radiation, so the magnetic transitions are not considered in our fit.

Channel	Q (MeV)	R (fm)	$l_{\max}$	Data
$\alpha + {}^{12}$C	0.000	6.5	6	AD,[a] ^{16}N
$\gamma_0 + {}^{16}O_0$	7.162	6.5	3	AD, $S_{\text{g.s.}}$
$\gamma_1 + {}^{16}O_1$	1.113	6.5	1	$S_{6.05}$
$\gamma_2 + {}^{16}O_2$	1.032	6.5	1	$S_{6.13}$
$\gamma_3 + {}^{16}O_3$	0.245	6.5	1	$S_{6.92}$
$\gamma_4 + {}^{16}O_4$	0.045	6.5	1	$S_{7.12}$
$\alpha_1 + {}^{12}$C	−4.438	6.5	2	AD, σ
$p + {}^{15}$N	−4.968	6.5	2	AD

[a]"AD" is the abbreviation for angular distribution.

B. Evaluation of experimental data

The basic principle of the data evaluation is that the database can reflect the information of nuclear structure and nuclear reactions accurately and objectively, no matter which is used: the original data or the appropriate amendment. R-matrix fitting requires experimental data covering the full energy region with complete energy points and continuous values, especially in the resonance-peak area with the different types of data. Reliable experimental data subsets should satisfy the following requirements: In the resonance-peak area, the sum of S factors in different reaction channels should be equal to the total S factor. The peak position of the different types of data should be consistent within the range of error. The principal value of different groups should be consistent within the range of uncertainty. The width data of resonance peaks are matched to the implied width information of the other data. The integral value of the differential data should be equal to the corresponding integral data. The integral data of different groups should span a broad energy range with a number of data points and have a good match with each other.

According to the principle of maximum likelihood, a fit to a dataset with many types and a large number of points needs to meet the approximate statistical distribution, so the revisions of some dataset are reasonable. If one experimental point obviously deviates from the expectations, such as the residual error being larger than three times the uncertainty, the error of this point can be enlarged by using Letts' criteria (3σ criteria). In the same type of data, if the difference of the principal value is far greater than their uncertainties, the error in the corresponding data should be amplified in the fitting. If the principal value in one group of data wholly deviates from the expected value, the normalization to this dataset is needed in the fitting. If one high-precision dataset is selected as the standard data in the evaluation, then some data with systematic deviation should be normalized to the standard data.

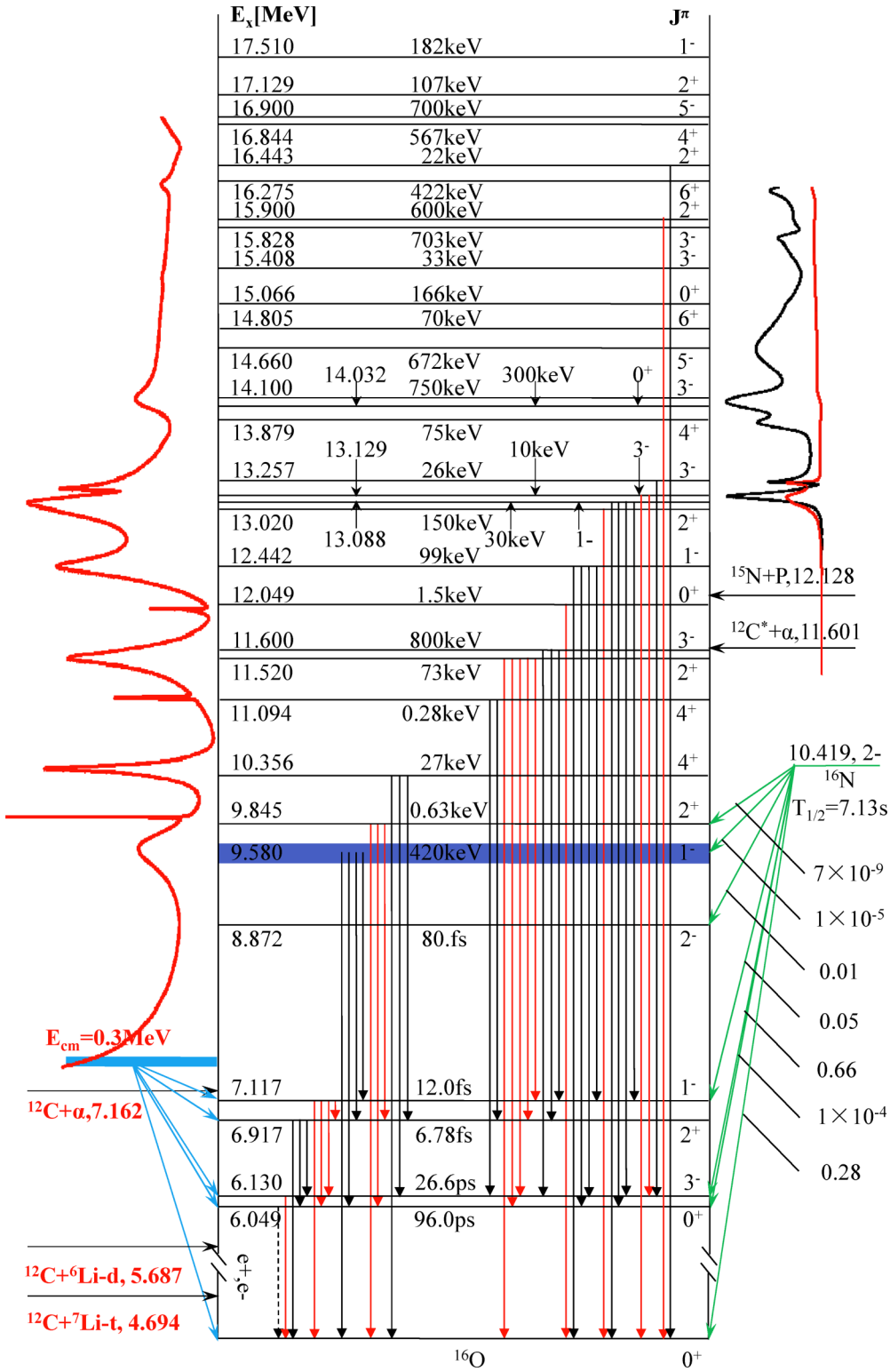

FIG. 2. (Color online) Level scheme of the ^{16}O nucleus [60]. All states relevant for the analysis are indicated.

C. Iterative fit

The fits to the data of ^{16}O system are iterated to achieve internal consistency. A file is a fixed record of the original data, which is to provide the original statistical error for the fit. Another file is a dynamic data file recording the evaluation process, whose role is to provide the actually-used data in fitting and which is updated in the iterative process. In the

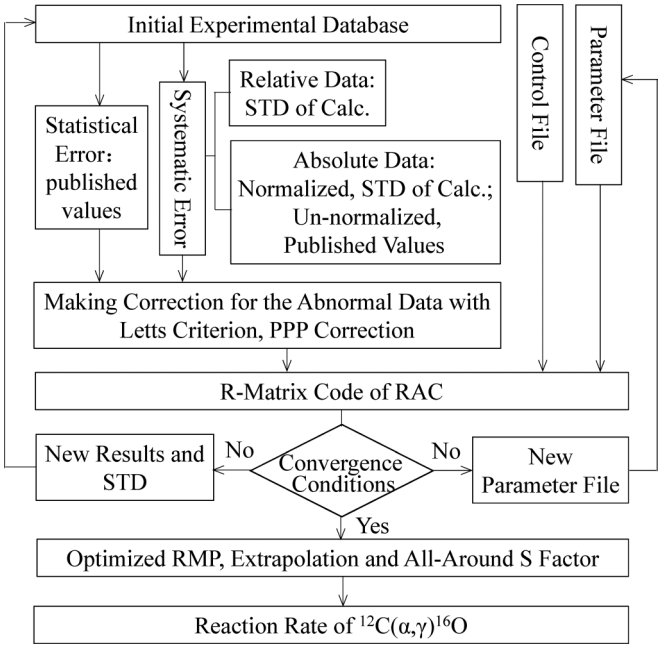

FIG. 3. The flow chart for the procedure of the iterative fit.

file the original relative data values are replaced with the new normalized value, and the systematic-error values are updated by the standard deviation (STD) of the new calculation. And the statistical errors are renewed with the original one at the beginning, but some of them are corrected according to Letts' criteria. The ratio of the corresponding data in there two files is the new scaling factor or normalization coefficient. The scaling factor is adjustable in the RAC, which is recorded in the parameter file together with the new R-matrix parameters. Figure 3 shows the flow chart for the R-matrix iterative fit procedure.

With the continuity of iterative fit, the variation of scaling factor becomes smaller and smaller, and the principal values of relative experimental data are closer to their expectations. Similarly, the R-matrix parameters (RMPs), fit values, and their standard deviations become more accurate. Finally, all calculated values tend to very slight fluctuations, and χ^2 approaches the minimum.

IV. RESULTS AND DISCUSSION

The following sections give details of the different reaction channels included in this analysis. Although they are described individually, the fits to the different reaction channel data sets have been performed simultaneously. Table III of Appendix A lists the different data sets which had free cross-section normalizations along with the normalization factor that was multiplied by the original scale. The R-matrix parameters of the channels which characterize the cross section in the figures are summarized in Table IV of Appendix B.

A. The reduced α-width amplitude for the bound states

At energies of astrophysical interest, direct cross-section measurements of capture reactions, such as $^{11}B(p,\gamma)^{12}C$, is very difficult because of the Coulomb barrier, but it can be derived by the proton spectroscopic factor and asymptotic normalization coefficients (ANCs) from the transfer reaction $^{12}C(^{11}B, ^{12}C)^{11}B$ [61] based on distorted wave Born approximation (DWBA) analysis [62–64]. The S factor of $^{12}C(\alpha,\gamma)^{16}O$ at astrophysical energies arises largely from the high-energy tails of subthreshold states 2_1^+ ($E_x = 6.92$ MeV) and 1_1^- ($E_x = 7.12$ MeV) of ^{16}O, but the properties of these states are only weakly constrained by cross-section measurements at higher energies. The cross sections of transfer reactions (^{6}Li,d) and (^{7}Li,t) provide an alternative way to extract the reduced α widths for these states of ^{16}O. In this fit, the γ_α of 1_1^- and 2_1^+ bound states are fixed to the weighted average of two new measurements [30,31], and the other subthreshold states, the γ_α of 0_1^+ and 3_1^- are adopted by the literature value of Ref. [31]. While the γ_γ of the four states could vary within their uncertainties in the literature [60].

B. Total S factor

The available total S factors of $^{12}C(\alpha,\gamma)^{16}O$ have been obtained in four independent experiments [7–10]. Figure 4 illustrates the corresponding fit values. In general, the fits are perfect when all the energy levels are accurately described. The measurement of Schürmann *et al.* [7,8] in inverse kinematics using the recoil mass separator ERNA allowed to collect data with high precision in a wide energy range, which would make a good restriction to the extrapolation of ground transitions, cascade transitions, and the total S factor. The data of Ref. [7] have not given definite numerical values for the three narrow peaks 2_2^+, 4_1^+, and 0_2^+, and the author's personal communication considers that the relative numerical value is difficult to be determined, so the excitation energies and partial widths are fixed by including in the dataset of pseudo-cross-section points which were assigned by 50% errors around the resonance peaks.

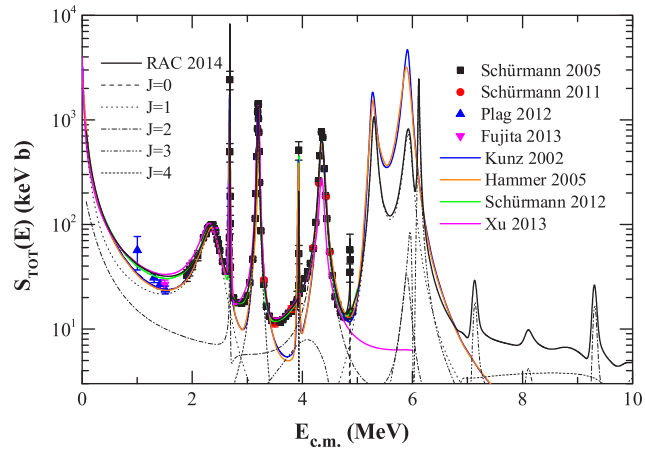

FIG. 4. (Color online) Results of the best R-matrix fit for the S_{tot} data from Schürmann 2005 [7], Schürmann 2011 [8], Plag 2012 [9], and Fujita 2013 [10], together with the decomposition into different energy-level contributions. For comparison, the results of Kunz 2002 [65], Hammer 2005 [43], Schürmann 2012 [40], and Xu 2013 [66] are also shown, respectively.

In the peak region of the 1_2^- energy level ($E_x = 9.58$ MeV), the evaluation of the data is as follows: We can learn the $S_{\rm tot} \approx 97.0$ keV b from the measurement of Schürmann *et al.* [7]. The evaluated $S_{\rm g.s.} \approx 76.0$ is from six groups of $S_{\rm g.s.}$. Estimating $S_{6.05} \approx 1.0$ keV b, $S_{6.92} \approx 7.0$ keV b, and $S_{7.12} \approx 20.0$ keV b from Refs. [15,24] and making assumption for $S_{6.13} \approx 1.0$ keV b. In view of the above, the sum of the partial S factor is 105 keV b, which is 1.08 times the result $S_{\rm tot} = 97$ keV b from the measurement of Schürmann *et al.* [7]; that is to say, the experimental value of the total S factor is significantly less than the sum of the experimental partial S factor. Relevant Ref. [7] accounts for that the maximal systemical error is 6.5%, so we choose 1.03 as the normalization coefficient of the data [8] in the careful exploration, then the data become $S_{\rm tot} = 100$ keV b, which is lower than the sum of partial S factors. The systematical study shows that the $S_{6.92}$ of Ref. [15] has an increasing trend, and the $S_{7.12}$ of this paper has a decreasing trend. When taking the normalization coefficient of $S_{6.92}$ and $S_{7.12}$ as 1.00 and 0.95, respectively, then the sum of partial S factors is approximately equal to 100 keV b. Therefore, we can get a satisfactory dataset which has complete types and numerical self-consistency for the main resonance peak 1_2^-. These constitute the skeleton of the whole database for the fits.

Another skeleton of the dataset is the data on the peak region of 2_3^- at $E_{\rm c.m.} = 4.358$ MeV (see Fig. 4). The data of Schürmann *et al.* [8] is obtained by adding their components $S_{\rm g.s.}$, $S_{6.05}$, $S_{6.13}$, $S_{6.92}$, and $S_{7.12}$, and it is very consistent with the total S factor of Schürmann *et al.* [7]. All kinds of data from Ref. [8] are used as the standard data, and the normalization coefficient is 1.03.

Recently, the $^{12}{\rm C}(\alpha,\gamma)\,^{16}{\rm O}$ cross sections of Plag *et al.* [9] have been measured at four energy points with $E_{\rm c.m.}$ between 1.00 and 1.51 MeV, and the $E10$ and $E20$ components were derived with an accuracy comparable to the previous best data obtained with HPGe detectors. These data are first employed in the $S_{\rm tot}$ fit, which have great influence on $S_{\rm tot}(0.3\ {\rm MeV})$. In Ref. [10], total-cross-section measurements for $E_{\rm c.m.} = 2.4$ and 1.5 MeV were performed at the Kyushu University Tandem accelerator Laboratory (KUTL) by using a tandem accelerator. And our fit results are relatively close to the principal values.

In current research on S factors of Refs. [43,65] at higher energies, i.e., at $E_{\rm c.m.} > 2.8$ MeV, resonance parameters taken from Ref. [60] were used in their R-matrix fit, in which the published data at high energy, such as α-capture measurements of Ref. [67], were neglected. So the high-energy resonances from $E_{\rm c.m.} = 5$ MeV to $E_{\rm c.m.} = 6$ MeV are apparently overestimated (please see fit of $S_{\rm g.s.}$). In addition, one should note that, in the analysis of Refs. [43,65], there is a clear disagreement at energies around $E_{\rm c.m.} = 3$ and 4 MeV, where the calculation underestimates the total cross section. The latest results of Ref. [40] are consistent with the available experimental data, but the high-energy data are not analyzed in a similar way as the R-matrix fit. In Ref. [66] (NACREII), the total and partial S factors are analyzed with the potential model, where the S factor at 2_3^+ ($E_x = 11.52$ MeV) is underestimated by the calculation.

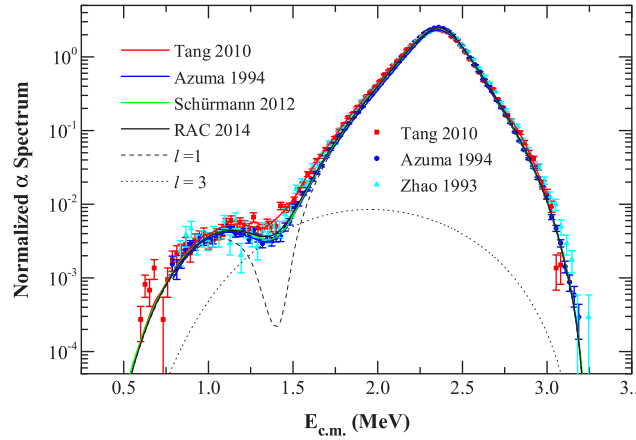

FIG. 5. (Color online) Results of the best R-matrix fits (black line) for the ^{16}N α spectra from Tang 2010 [26], Azuma 1994 [27], and Zhao 1993 [28], together with the decomposition into p- (dashed line) and f-wave (dotted line) contributions. For comparison, the best fits of Tang 2010 [26], Azuma 1994 [27], and Schürmann 2012 [40] are shown, scaled by the corresponding coefficients.

C. ^{16}N α spectrum

The shape of the low-energy part of the β-delayed α spectrum of ^{16}N is very sensitive to the $\alpha + {}^{12}$C reduced width of the 1_1^- subthreshold state and 1_2^- state of ^{16}O, which, in turn, dominates the low-energy p-wave capture $S_{E10}(0.3\ {\rm MeV})$ of $^{12}{\rm C}(\alpha,\gamma_0)\,^{16}{\rm O}_0$. In this energy region the reduced α widths are determined by the α spectra and the angular distributions of $^{12}{\rm C}(\alpha,\alpha)\,^{12}{\rm C}$, which results in competition with each other in the fit. As shown in Ref. [68], there exists a limitation by the use of $^{12}{\rm C}(\alpha,\alpha)\,^{12}{\rm C}$ data in Ref. [32] for obtaining reliable values of $S_{E10}(0.3\ {\rm MeV})$. So the ^{16}N α spectrum may help to give a better confirmation of the reduced α width amplitude of 1_1^- and 1_2^-. Included in this analysis are the three independent α spectra data of Refs. [25–28], and the normalization for probability spectrum is used in the practice to reduce the influence of systematical errors. Figure 5 shows the fit to the normalized ^{16}N α spectrum together with the decomposition into p- and f-wave contributions, which suggests a significantly negative interference of the bound 1_1^- state with the broad 1_2^- state that leads to a second peak at $E_{\rm c.m.} = 1.1$ MeV and a minimum in the vicinity of 1.4 MeV. The dotted line denotes the contribution of 3^- state, which perfectly compensates this negative interference. The fit concluded that the measurement of Azmua *et al.* [27] most likely represents the current closest approximation to the true α spectrum.

D. $^{12}{\rm C}(\alpha,\gamma_0)\,^{16}{\rm O}_0$

For the ground-state transitions, the secondary data of E_{10} and E_{20} multipoles were used in the previous R-matrix analysis independently [40,50]. In general, these secondary data were obtained from the Legendre polynomials fit [11] (page 510) to the angular distributions of $^{12}{\rm C}(\alpha,\gamma_0)\,^{16}{\rm O}_0$ measured at many discrete energies. Two methods of analysis (phase fixed or free) are often applied; however, the derived S factors S_{E10} and S_{E20} are significantly different for the same

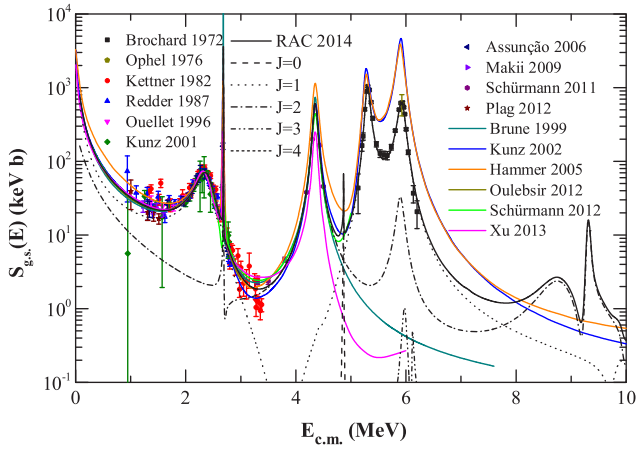

FIG. 6. (Color online) Results of the best R-matrix fits for the ground-state transitions $S_{\text{g.s.}}$ data from Brochard 1972 [67], Ophel 1976 [20], Kettner 1982 [23], Redder 1987 [12], Ouellet 1996 [13], Kunz 2001 [15], Assunção 2006 [16], Makii 2009 [18], Schürmann 2011 [8], and Plag 2012 [9], together with the decomposition into different energy-level contributions. For comparison, the results of Brune 1999 [29], Kunz 2002 [65], Hammer 2005 [43], Schürmann 2012 [40], Oulebsir 2012 [31], and Xu 2013 [66] are shown.

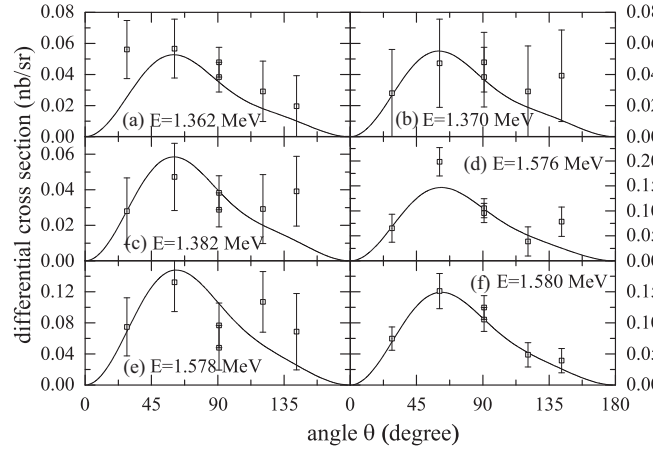

FIG. 7. Fits to the $^{12}C(\alpha,\gamma_0)\,^{16}O_0$ angular distributions of Ouellet 1996 [13] at (a) $E_{\text{c.m.}} = 1.362$, (b) 1.370, (c) 1.382, (d) 1.576), (e) 1.578, and (f) 1.580 MeV.

γ angular distributions; see Fig. 12 of Ref. [16], especially for S_{E20}.

In our fit, $S_{\text{g.s.}} = S_{E10} + S_{E20}$ is used for the ground-state transition, from which the proportion of S_{E10} and S_{E20} are determined by the R-matrix fit to the relevant γ angular distributions. Figure 6 show the fit to the $^{12}C(\alpha,\gamma_0)\,^{16}O_0$ data of ten independent measurements and the calculations of previous works. After the experiments by Dyer and Barnes [11], Kettner *et al.* [23], and Redder *et al.* [12], a weighted average value σ of 47 ± 3 nb at a resonance peak of 1_2^- was used to derive a cross section at low energy; these data play a vital role for the determination of $S_{\text{g.s.}}$ and can be regarded as a criterion for normalizing the experimental data. Even though $S_{\text{g.s.}}$ of Kettner *et al.* [23] deviates systematically from the other data in this resonance region, it is dispensable since it is the only one that has the data points above 3.0 MeV. It is noteworthy that, if the normalization coefficient is fixed by a factor of 0.87, the data of the 1_2^- peak region is consistent with the other data; meanwhile the data above 3.0 MeV is well consistent with $S_{\text{g.s.}}$ of Schürmann *et al.* [8].

In the higher-energy region, there are five independent experiments [19–22,67] covering 1_3^- ($E_x = 12.44$ MeV) and 1_4^- ($E_x = 13.09$ MeV). All the available measurements of the relative ratio of peak cross sections $\sigma(1_3^-)/\sigma(1_4^-)$, are tabulated in Table 3 of Ref. [20], in which the largest deviation of Ref. [67] data from the other three data sets, lower by about 20%, are evident. So in our fit, the data of Ref. [67] near the 1_4^- resonance are corrected to the data at the peak of 1_3^- with a factor 0.81. Then the cross sections are found to be in a good agreement with the absolute data from Ref. [20] if normalization corrections (maximum of $\pm 20\%$) are applied. The remaining data from Refs. [19,21,22] show good agreement in the shape of the excitation curves, and the normalization factors are given in Table III.

The corresponding R-matrix calculation of angular distributions for the reaction $^{12}C(\alpha,\gamma_0)\,^{16}O_0$ is illustrated in Figs. 7 to 20 at representative α energies from $E_{\text{c.m.}} = 1.002$ to $E_{\text{c.m.}} = 6.075$ MeV. The angular distribution measured at the 2_2^+ ($E_x = 9.84$ MeV) has the familiar $E20$ pattern and is symmetric with respect to 90°, while the distributions obtained at other energies are asymmetric about 90°, clearly indicating the presence of both $E10$ and $E20$ amplitudes in the capture mechanism. With the much-improved γ-ray angular distributions in our R-matrix calculation, it is now possible to derive more accurate values for the cross sections of the E_{10} and E_{20} transitions to the ground state of ^{16}O. Figures 21 and 22 show the calculations of S_{E10} and S_{E20} together with all available experimental data. Although the data of S_{E10} and S_{E20} are not used in the fits, these data lie uniformly on two sides of our calculation, which in turn illustrates the

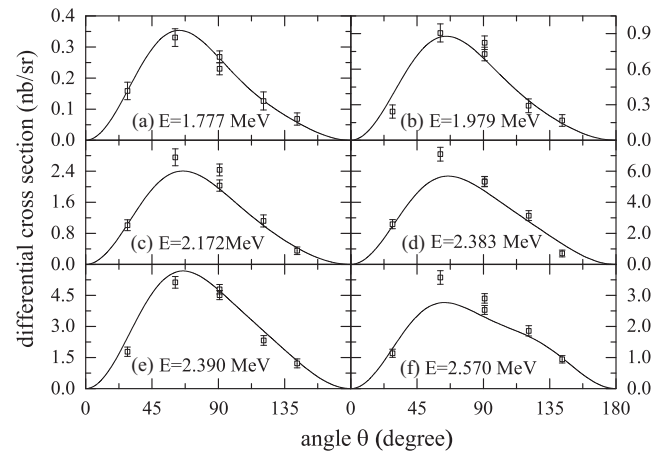

FIG. 8. Fits to the $^{12}C(\alpha,\gamma_0)\,^{16}O_0$ angular distributions of Ouellet 1996 [13] at (a) $E_{\text{c.m.}} = 1.777$, (b) 1.979, (c) 2.172, (d) 2.383, (e) 2.390, and (f) 2.570 MeV.

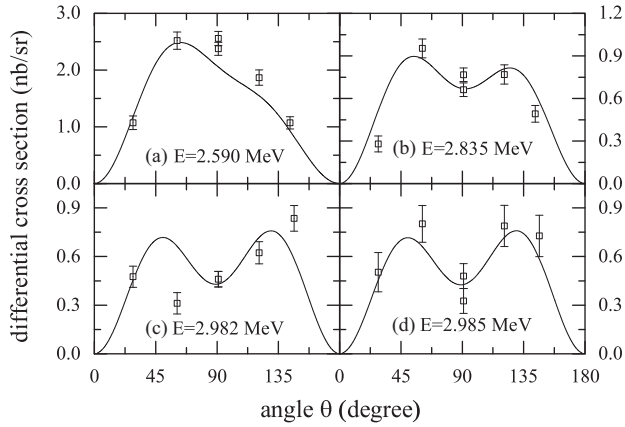

FIG. 9. Fits to the $^{12}C(\alpha,\gamma_0)^{16}O_0$ angular distributions of Ouellet 1996: [13] at (a) $E_{c.m.} = 2.590$, (b) 2.835, (c) 2.982, and (d) 2.985 MeV.

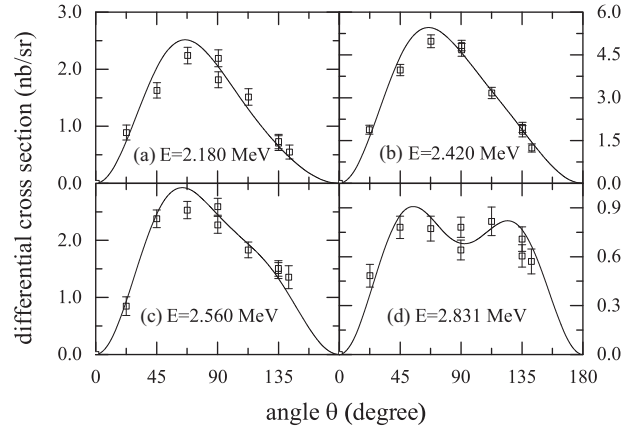

FIG. 11. Fits to the $^{12}C(\alpha,\gamma_0)^{16}O_0$ angular distributions of Dyer 1974 [11] at (a) $E_{c.m.} = 2.180$, (b) 2.420, (c) 2.560, and (d) 2.831 MeV.

rationality and self-consistency in our R-matrix fit of the angular distributions and $S_{g.s.}$, ground-state transitions.

In Refs. [13,70] the 1^-_1 subthreshold state and the 1^-_2 resonance may interfere destructively and result in a significantly lower S_{E10}. However, the constructive solution is strongly favored and the destructive interference pattern has been eliminated in our calculation of angular distribution, resulting in a value of $S_{E10}(0.3\ \text{MeV}) = 98.0 \pm 7.0$ keV b.

The cross section around the $E_{c.m.} = 2.5-3.0$ MeV region is a rapidly changing function of energy, which strongly depends upon the interference scheme between the resonance 2^+_2 and other E_{20} amplitudes. But the relative E_{20}–E_{20} interference sign is not well determined by the integrated capture data, i.e., the best result of Ref. [40] in an interference pattern determined by the high-energy data of Ref. [8] is different from most previous analyses [65,71]. The interference scheme has been commendably constrained by the angular distributions calculation in our R-matrix fitting near this resonance, which are in accordance with the new

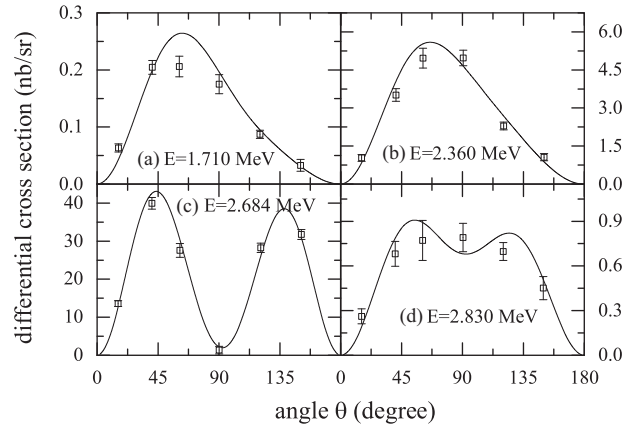

FIG. 12. Fits to the $^{12}C(\alpha,\gamma_0)^{16}O_0$ angular distributions of Redder 1987 [12] at (a) $E_{c.m.} = 1.710$, (b) 2.360, (c) 2.684, and (d) 2.830 MeV.

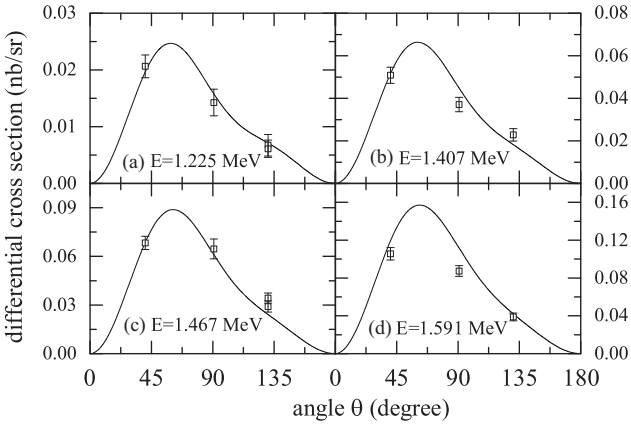

FIG. 10. Fits to the $^{12}C(\alpha,\gamma_0)^{16}O_0$ angular distributions of Makii 2009 [18] at (a) $E_{c.m.} = 1.225$, (b) 1.470, (c) 1.467, and (d) 1.591 MeV.

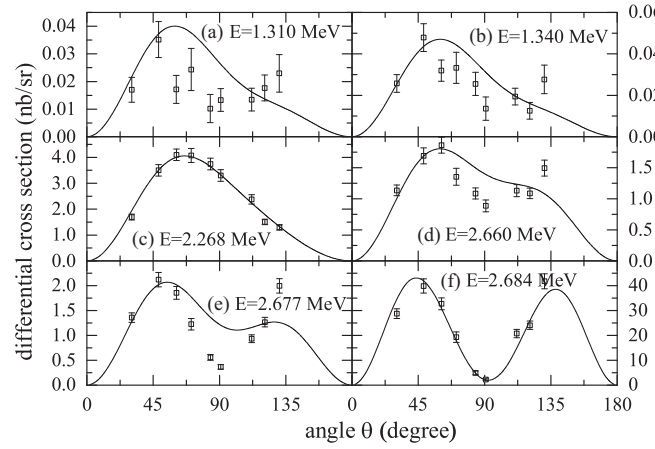

FIG. 13. Fits to the $^{12}C(\alpha,\gamma_0)^{16}O_0$ angular distributions of Assunção 2006 [16] at (a) $E_{c.m.} = 1.310$, (b) 1.340, (c) 2.268, (d) 2.660, (e) 2.677, and (f) 2.684 MeV.

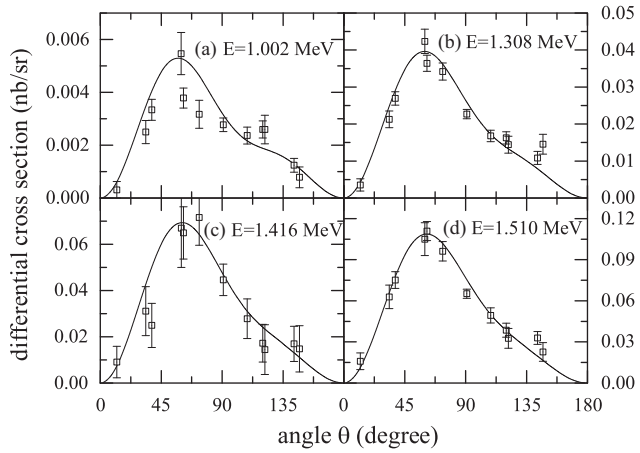

FIG. 14. Fits to the $^{12}C(\alpha,\gamma_0)^{16}O_0$ angular distributions of Plag 2012 [9] at (a) $E_{\text{c.m.}} = 1.002$, (b) 1.308, (c) 1.416, and (d) 1.510 MeV.

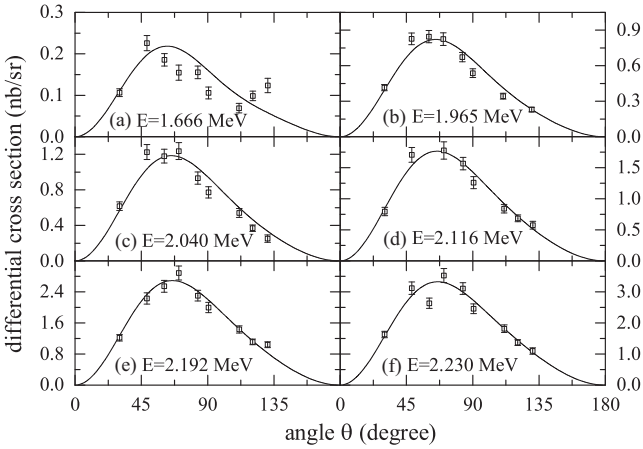

FIG. 15. Fits to the $^{12}C(\alpha,\gamma_0)^{16}O_0$ angular distributions of Fey 2004 [17] at (a) $E_{\text{c.m.}} = 1.666$, (b) 1.965, (c) 2.040, (d) 2.116, (e) 2.192, and (f) 2.230 MeV.

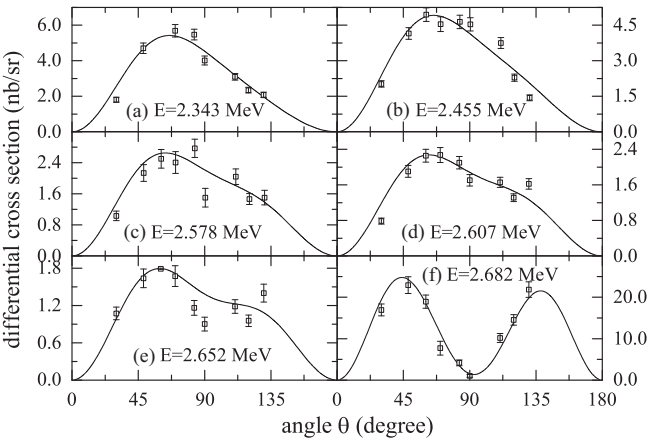

FIG. 16. Fits to the $^{12}C(\alpha,\gamma_0)^{16}O_0$ angular distributions of Fey 2004 [17] at (a) $E_{\text{c.m.}} = 2.343$, (b) 2.455, (c) 2.578, (d) 2.607, (e) 2.652, and (f) 2.682 MeV.

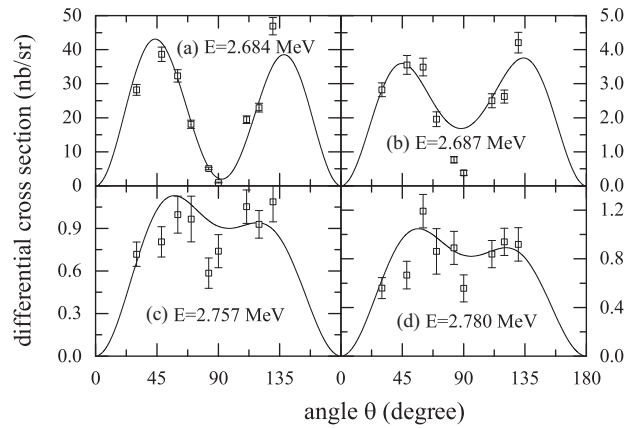

FIG. 17. Fits to the $^{12}C(\alpha,\gamma_0)^{16}O_0$ angular distributions of Fey 2004 [17] at (a) $E_{\text{c.m.}} = 2.684$, (b) 2.687, (c) 2.757, and (d) 2.780 MeV.

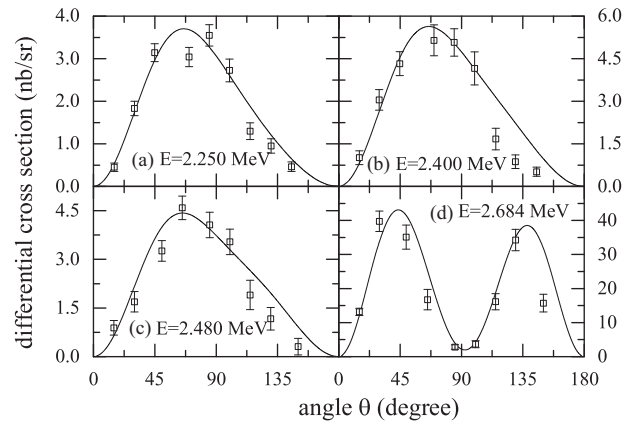

FIG. 18. Fits to the $^{12}C(\alpha,\gamma_0)^{16}O_0$ angular distributions of Kunz 1997 [14] at (a) $E_{\text{c.m.}} = 2.250$, (b) 2.400, (c) 2.480, and (d) 2.684 MeV.

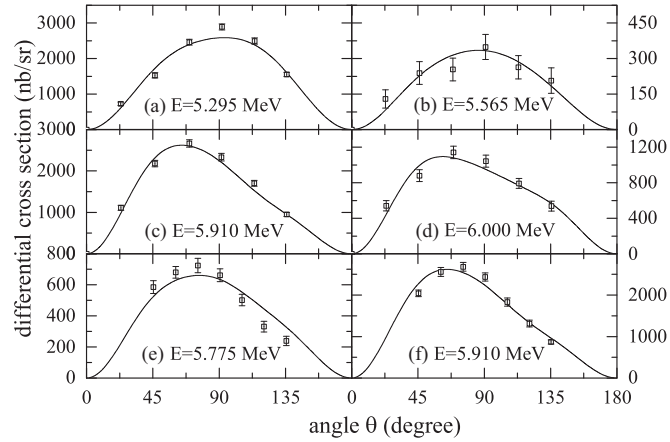

FIG. 19. Fits to the $^{12}C(\alpha,\gamma_0)^{16}O_0$ angular distributions of Larson 1964 [19] and Kernel 1971 [21] at (a) $E_{\text{c.m.}} = 5.295$, (b) 5.565, (c) 5.910, (d) 6.000, (e) 5.775, and (f) 5.910 MeV.

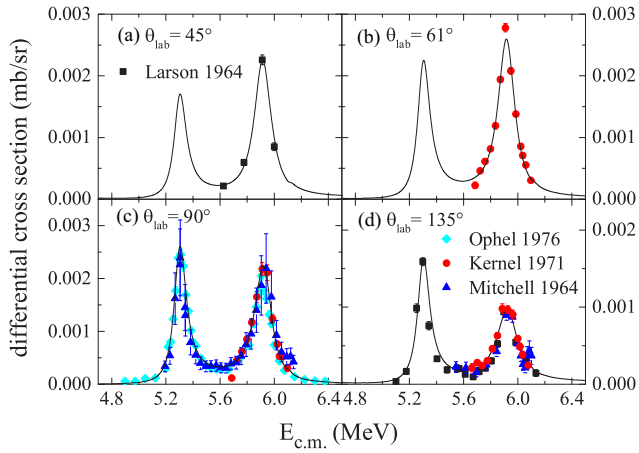

FIG. 20. (Color online) Fits to the $^{12}C(\alpha,\gamma_0)^{16}O_0$ differential cross-section data at (a) 45°, (b) 61°, (c) 90°, and (d) 135° from Larson 1964 [19], Kernel 1971 [21], Ophel 1976 [20], and Mitchell 1964 [22].

measurement result of Ref. [41], and the extrapolation values of $S_{E20}(0.3\ \text{MeV}) = 56.0 \pm 4.1$ keV b in our calculation.

E. $^{12}C(\alpha,\gamma_1)^{16}O_1$

Radiative α-particle capture into the first-excited $J^\pi = 0^+$ state at 6.05 MeV excitation energy has been investigated recently in two independent experiments [8,24]; however, there exists big differences between their results for $S_{6.05}(0.3\ \text{MeV})$. So it is necessary to give a detailed research and discussion. In the work of Matei *et al.* [24], $S_{6.05}(0.3\ \text{MeV}) = 25^{+25}_{-16}$ keV b is obtained by fitting the experimental results therein. It mainly comes from S_{E1} and partially from S_{E2} and is with large

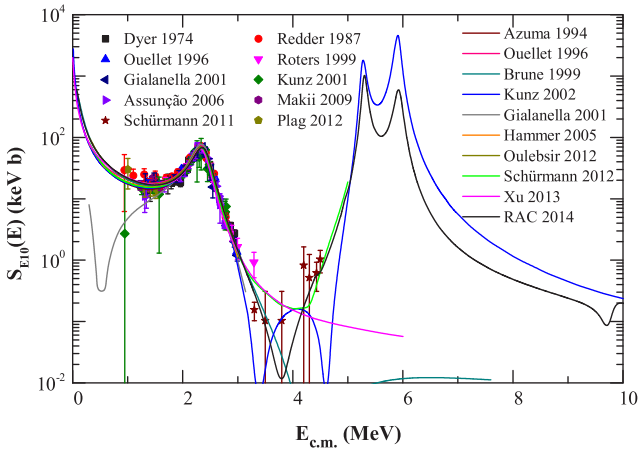

FIG. 21. (Color online) Calculation of S_{E10} with the best R-matrix fit. For comparison, previous fits of Azuma 1994 [27], Ouellet 1996 [13], Brune 1999 [29], Gialanella 2001 [70], Kunz 2002 [65], Hammer 2005 [43], Schürmann 2012 [40], Oulebsir 2012 [31], and Xu 2013 [66] are shown. Data points shown are taken from Dyer 1974 [11], Redder 1987 [12], Ouellet 1996 [13], Roters 1999 [69], Kunz 2001 [15], Gialanella 2001 [70], Assunção 2006 [16], Makii 2009 [18], Schürmann 2011 [8], and Plag 2012 [9].

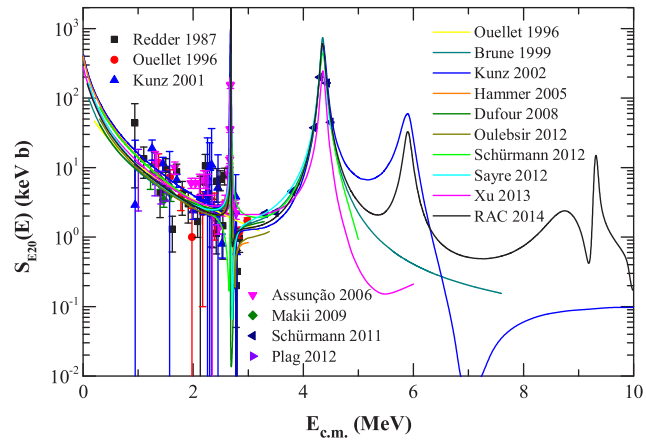

FIG. 22. (Color online) Calculation of S_{E20} with the best R-matrix fit. For comparison, previous fits of Ouellet 1996 [13], Brune 1999 [29], Kunz 2002 [65], Hammer 2005 [43], Dufour 2008 [71], Oulebsir 2012 [31], Schürmann 2012 [40], Sayre 2012 [41] and Xu 2013 [66] are shown. Data points shown are taken from Redder 1987 [12], Ouellet 1996 [13], Kunz 2001 [15], Assunção 2006 [16], Makii 2009 [18], Schürmann 2011 [8], and Plag 2012 [9].

error. In contrast with the analysis of Ref. [24], and the extrapolation of Ref. [8] suggests a negligible contribution from this amplitude, $S_{6.05}(0.3\ \text{MeV}) < 1$ keV b by analyzing their data, which is mainly contributed by S_{E2} and little by S_{E1}. References [8,24] use the same experimental method, and both their original data show the γ contribution of the first-excited state (0^+_1, 6.05 MeV). But Ref. [8] concludes that the $S_{6.05}$ is negligible in the energy region less than 3.3 MeV, so it only gives the experimental data above this energy (see Fig. 23).

In our fit, the data of Ref. [8] are regarded as standard data and the normalization coefficient is 1.03. The energy regions of the data in Refs. [8,24] overlap around 3.5 MeV. The data of Ref. [24] can be normalized by that of Ref. [8], and the

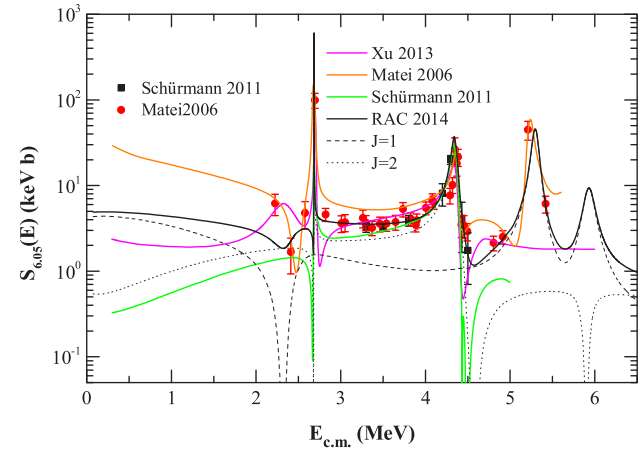

FIG. 23. (Color online) Results of best R-matrix fit for the cascade transitions $S_{6.05}$ from Schürmann 2011 [8] and Matei 2006 [24], together with the decomposition into different energy-level contributions. For comparison, the results of Schürmann 2011 [8], Matei 2006 [24], and Xu 2013 [66] are shown in this figure.

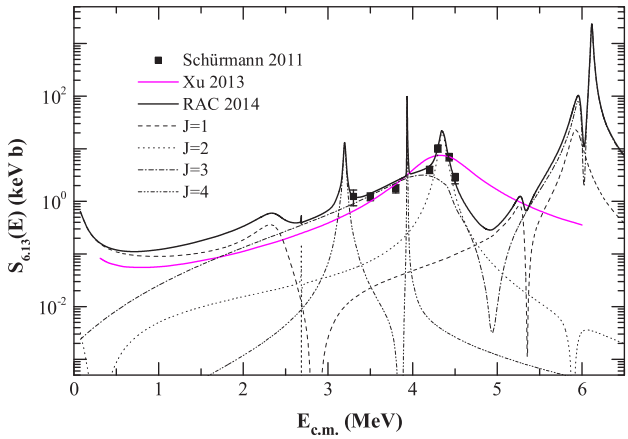

FIG. 24. (Color online) Results of the best R-matrix fit for the cascade transitions $S_{6.13}$ from Schürmann 2011 [8] together with the decomposition into different energy-level contributions. For comparison, the result of Xu 2013 [66] is shown in this figure.

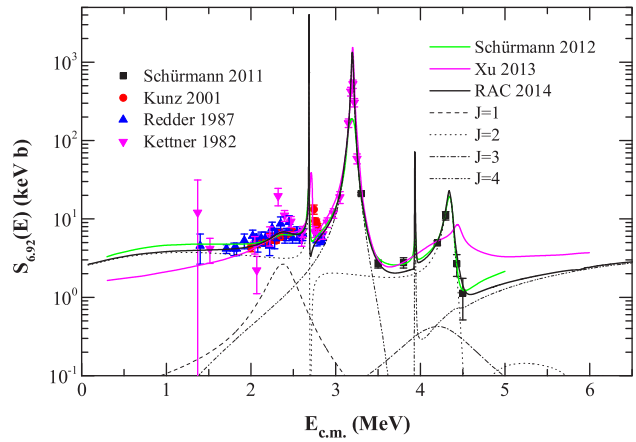

FIG. 25. (Color online) Results of the best R-matrix fit for the cascade transitions $S_{6.92}$ from Redder 1987 [12], Kettner 1982 [23], Kunz 2001 [15], and Schürmann 2011 [8], together with the decomposition into different energy-level contributions. For comparison, the results of Schürmann 2012 [40] and Xu 2013 [66] are shown in this figure.

normalization factor is 0.88. This forms a dataset of $S_{6.05}$ which covers the full energy region with complete energy points and continuous values. This transition can therefore be estimated to be $S_{6.05}(0.3\ \text{MeV}) = 4.9 \pm 1.2$ keV b, where S_{E1} is the most important contribution in $S_{6.05}(0.3\ \text{MeV})$. The result for $S_{6.05}$ obtained by this work is from the systematic analysis of the whole ^{16}O system. Hence, compared with previous analyses, our result is much more firmly based on the experiments and is reliable.

F. ^{12}C(α,γ_2)^{16}O$_2$

Very little data exists on the transition into the $E_x = 6.13$ MeV state ($J^\pi = 3^-$) except for the 2_3^+ resonance at $E_x = 11.60$ MeV and the 3_2^- resonance at $E_x = 11.52$ MeV of Ref. [8]. The parameters of these resonance can be sufficient to describe this data and the fit result is $S_{6.13}(0.3\ \text{MeV}) = 0.2 \pm 0.1$ keV b (see Fig. 24).

G. ^{12}C(α,γ_3)^{16}O$_3$

Four cascade data sets of $S_{6.92}$ [8,12,15,23] cover a range from $E_{c.m.} = 1.4$ to 5.5 MeV, and the cross section at astrophysical energy is largely governed by the direct-capture process, from s-, d-, and g-wave captures in Refs. [8,12,23,42]. With the reasonable normalization of Refs. [12,23], a good fit to these experimental data is achieved from resonance parameters and a direct-capture parameter for $J^\pi = 2_1^+$ (see Tables IV), resulting in $S_{6.92}(0.3\ \text{MeV}) = 3.0 \pm 0.4$ keV b, which is consistent with the result of Ref. [40]. Figure 25 shows the results of $S_{6.92}$ as well as its decomposition into different level contributions. Also, the normalization factors are given in Table III.

H. ^{12}C(α,γ_4)^{16}O$_4$

The capture of $S_{7.12}$ would be expected to proceed mainly via p- and f-wave direct process and resonance transition at low energies [8,12]. With resonance parameters and a direct-capture parameter for $J^\pi = 1_1^-$, a good fit to the experimental data [8,12,15] is obtained (see parameter table). And the extrapolated S factor for this transition is also small, $S_{7.12}(0.3\ \text{MeV}) = 0.6 \pm 0.2$ keV b. The normalization factors of these applied data are given in Table III. Figure 26 shows the results of $S_{7.12}$ as well as its decomposition into different level contributions.

I. ^{12}C(α,α)^{12}C

The most widely used elastic-scattering data of α particles on ^{12}C contain the α particle information for all relevant states in ^{16}O, which can be obtained with rather high accuracy. Previous elastic-scattering data have been used to determine the scattering phase shifts for individual angular momenta [26,40] and so on. Such a procedure is necessary in cases when the analysis of ^{12}C(α,γ)^{16}O is restricted to

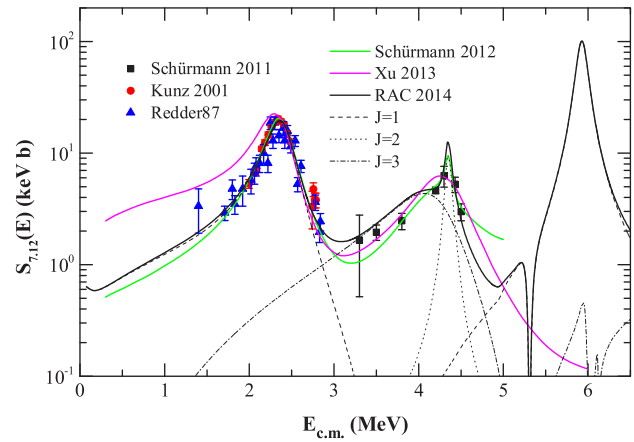

FIG. 26. (Color online) Results of the best R-matrix fit for the cascade transitions $S_{7.12}$ from Redder 1987 [12], Kunz 2001 [15], and Schürmann 2011 [8], together with the decomposition into different energy-level contributions. For comparison, the results of Schürmann 2012 [40] and Xu 2013 [66] are shown in this figure.

only one particular angular momentum, but the interference structures in all data, associated with all the resonance states, have been neglected [40,44]. Taking all angular momenta into account simultaneously, R-matrix fits of four groups of angular distributions and the associated data [32–36] are presented from $E_{\text{c.m.}} = 1.1$ to $E_{\text{c.m.}} = 5.85$ MeV in Figs. 27 to 38 with the strictly theoretical formulas of Eq. (19). In order to reduce the space of the paper, the figures from $E_{\text{c.m.}} = 5.85$ MeV to $E_{\text{c.m.}} = 7.5$ MeV of Refs. [35,36] are not shown in this paper.

The scattering data by Plaga *et al.* [32] were obtained in a considerably better energy range in comparison with the other studies. Differential-cross-section data for all 35 angles in the range $\theta_{\text{lab}} = 22^\circ$ to 163° and for 51 energies from $E_{\text{c.m.}} = 1.0$ to 4.9 MeV are included in the fit. Data points in the vicinity of narrow resonances are also contained for this analysis. Level parameters from the fit are in an excellent agreement with those reported in Ref. [60]. The interference structures in the data, associated with resonance states in the energy range covered by this data, are well reproduced by the R-matrix fits. All the results are shown in Figs. 27 to 35.

Recently, the angular distributions of $^{12}\text{C}(\alpha,\alpha)^{12}\text{C}$ in the α-energy range of 2.6–8.2 MeV, at angles from 24° to 166° have been measured at the University of Notre Dame using an array of 32 silicon detectors [33,34]. The relative differential-cross-section excitation curves for eight selected detector angles and the four angular distributions for energies near the $E_{\text{c.m.}} = 2.291(1_2^-)$, $3.192(4_2^+)$, $3.913(2_3^+)$, and $4.902(0_2^+)$ MeV resonances are available. To reduce the amount of computations, only the four angular distributions are employed in this fit, which the angular distributions are found to be in a good agreement with those data. Fits are shown in Fig. 36.

The best quality α-scattering cross-section data above proton separation energies are shown in Figs. 37 and 38 of Ref. [35], which have good coherence with experimental data.

J. $^{12}\text{C}(\alpha,\alpha_1)^{12}\text{C}$ and $^{12}\text{C}(\alpha,p)^{15}\text{N}$

Good fits of $^{12}\text{C}(\alpha,\alpha_1)^{12}\text{C}$ and $^{12}\text{C}(\alpha,p)^{15}\text{N}$ are helpful to reduce the uncertainty produced by the distant levels, and then to improve the fit precision of $^{12}\text{C}(\alpha,\gamma)^{16}\text{O}$ S factor subsequently. Previously, the only available angular distribution data of the $^{12}\text{C}(\alpha,\alpha_1)^{12}\text{C}$ reaction has been obtained at incident energies $E_{\text{c.m.}} = 5.963$, 6.015, and 6.105 MeV in Ref. [37]. And the excitation curves of $^{12}\text{C}(\alpha,\alpha_1)^{12}\text{C}$ and $^{12}\text{C}(\alpha,p)^{15}\text{N}$ for four selected detector angles have been measured in the same energy range in the paper. But an absolute scaling was not reported in these measurements. In Refs. [38,39], new yield-ratio data for the reactions $^{12}\text{C}(\alpha,\alpha_1)^{12}\text{C}$ and $^{12}\text{C}(\alpha,p)^{15}\text{N}$ were performed at the University of Notre Dame in order to provide additional data for a comprehensive R-matrix analysis of compound-nucleus reactions populating ^{16}O. The data are in the form of yield ratios where the $^{12}\text{C}(\alpha,\alpha_0)^{12}\text{C}$ yields measured at an angle $\theta_{\text{lab}} = 58.9^\circ$ are used as the reference data. The transformational angular distribution data and cross sections were obtained by a private communication with deBoer.

The R-matrix fits of the $^{12}\text{C}(\alpha,\alpha_1)^{12}\text{C}$ angle-integrated cross section are shown by the solid lines in Fig. 39, illustrating the consistency level of the simultaneous fit to the data of Ref. [38] together with the relative data in Ref. [37]. Fits of the available angular-distribution data are shown in Figs. 40 to Fig. 43, in which the significant contributions originate from states at $E_x = 12.95(2_4^+)$, $13.13(3_3^-)$, and $13.27(3_4^-)$ MeV. Fits for the angular distribution data of Ref. [37] for the reaction $^{12}\text{C}(\alpha,p)^{15}\text{N}$ are shown in Fig. 44, and the normalization factors are given in Table III.

V. SUMMARY

This study presents a new R-matrix theory for the $^{12}\text{C}(\alpha,\gamma)^{16}\text{O}$ S factor at helium-burning temperatures and a

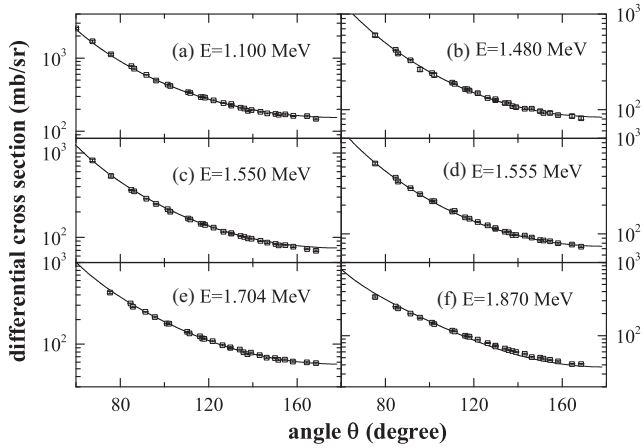

FIG. 27. Fits to the $^{12}\text{C}(\alpha,\alpha)^{12}\text{C}$ angular distributions of Plaga 1987 [32] at (a) $E_{\text{c.m.}} = 1.100$, (b) 1.480, (c) 1.550, (d) 1.555, (e) 1.704, and (f) 1.870 MeV.

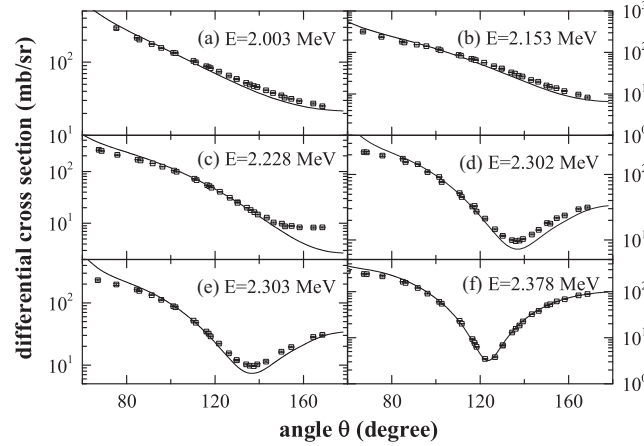

FIG. 28. Fits to the $^{12}\text{C}(\alpha,\alpha)^{12}\text{C}$ angular distributions of Plaga 1987 [32] at (a) $E_{\text{c.m.}} = 2.003$, (b) 2.153, (c) 2.228, (d) 2.302, (e) 2.303, and (f) 2.378 MeV.

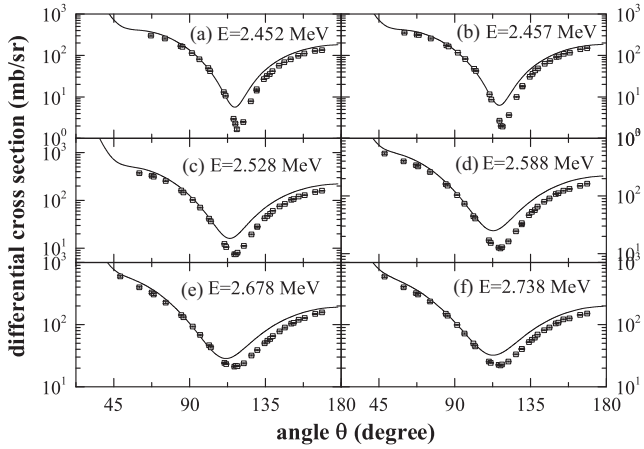

FIG. 29. Fits to the $^{12}C(\alpha,\alpha)^{12}C$ angular distributions of Plaga 1987 [32] at (a) $E_{c.m.} = 2.452$, (b) 2.457, (c) 2.528, (d) 2.588, (e) 2.678, and (f) 2.738 MeV.

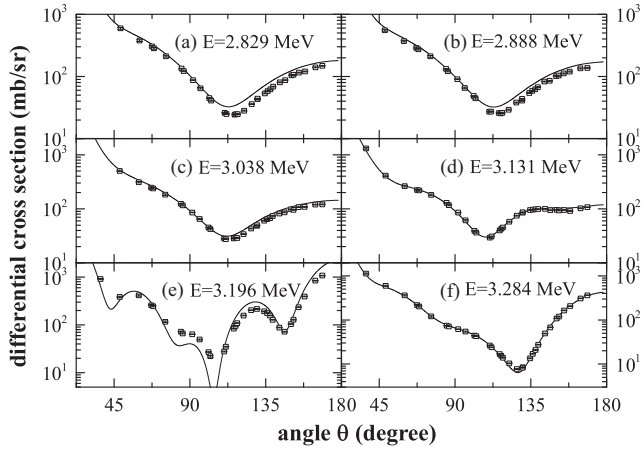

FIG. 30. Fits to the $^{12}C(\alpha,\alpha)^{12}C$ angular distributions of Plaga 1987 [32] at (a) $E_{c.m.} = 2.829$, (b) 2.888, (c) 3.038, (d) 3.131, (e) 3.196, and (f) 3.284 MeV.

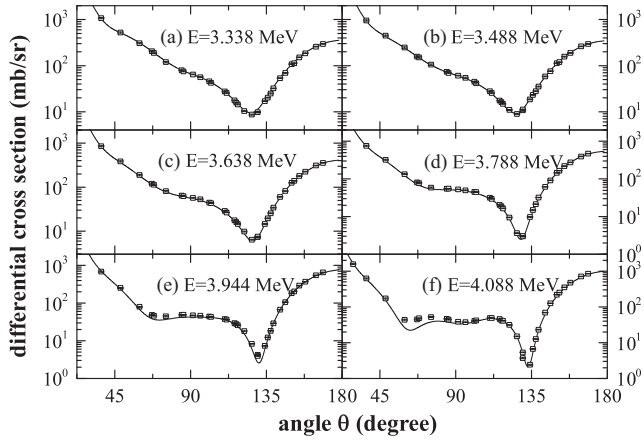

FIG. 31. Fits to the $^{12}C(\alpha,\alpha)^{12}C$ angular distributions of Plaga 1987 [32] at (a) $E_{c.m.} = 3.338$, (b) 3.488, (c) 3.638, (d) 3.788, (e) 3.944, and (f) 4.088 MeV.

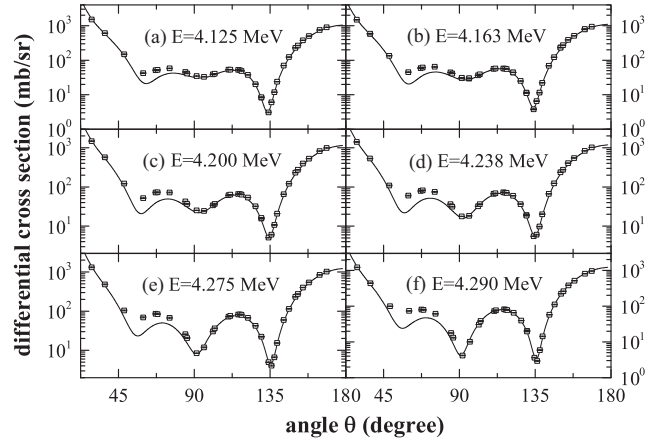

FIG. 32. Fits to the $^{12}C(\alpha,\alpha)^{12}C$ angular distributions of Plaga 1987 [32] at (a) $E_{c.m.} = 4.125$, (b) 4.163, (c) 4.200, (d) 4.238, (e) 4.275, and (f) 4.290 MeV.

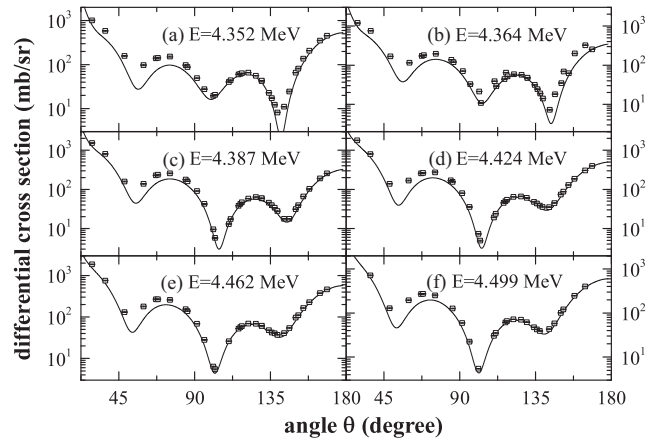

FIG. 33. Fits to the $^{12}C(\alpha,\alpha)^{12}C$ angular distributions of Plaga 1987 [32] at (a) $E_{c.m.} = 4.352$, (b) 4.364, (c) 4.387, (d) 4.424, (e) 4.462, and (f) 4.499 MeV.

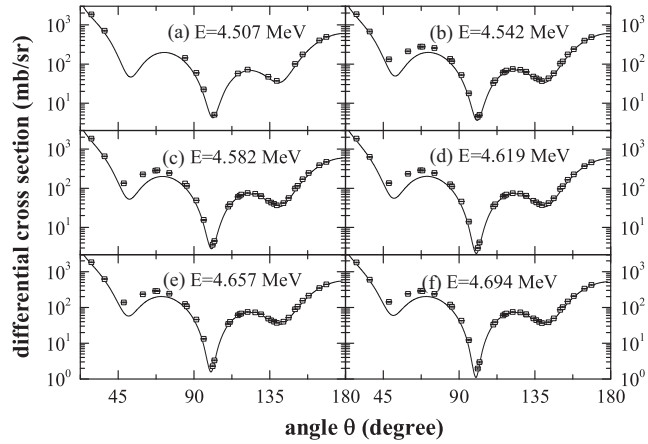

FIG. 34. Fits to the $^{12}C(\alpha,\alpha)^{12}C$ angular distributions of Plaga 1987 [32] at (a) $E_{c.m.} = 4.507$, (b) 4.542, (c) 4.582, (d) 4.619, (e) 4.657, and (f) 4.694 MeV.

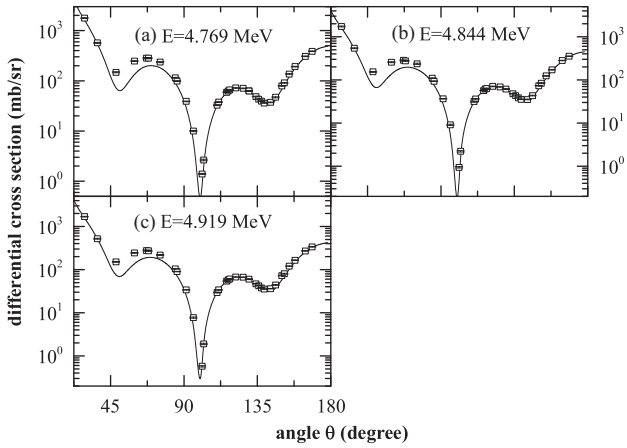

FIG. 35. Fits to the $^{12}C(\alpha,\alpha)^{12}C$ angular distributions of Plaga 1987 [32] at (a) $E_{c.m.} = 4.769$, (b) 4.844, and (c) 4.919 MeV.

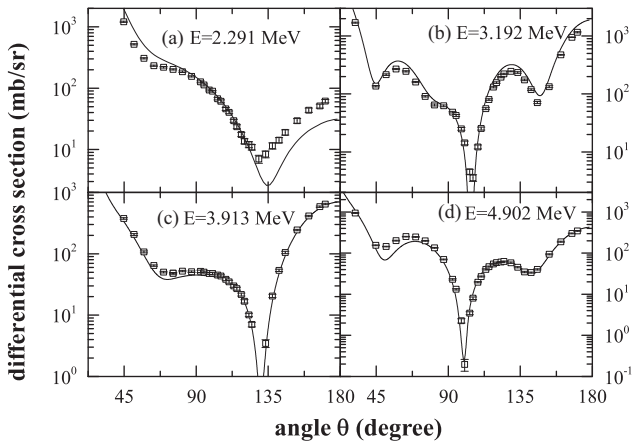

FIG. 36. Fits to the $^{12}C(\alpha,\alpha)^{12}C$ angular distributions of Tischhauser 2009 [34] at (a) $E_{c.m.} = 2.291$, (b) 3.192, (c) 3.913, and (d) 4.902 MeV.

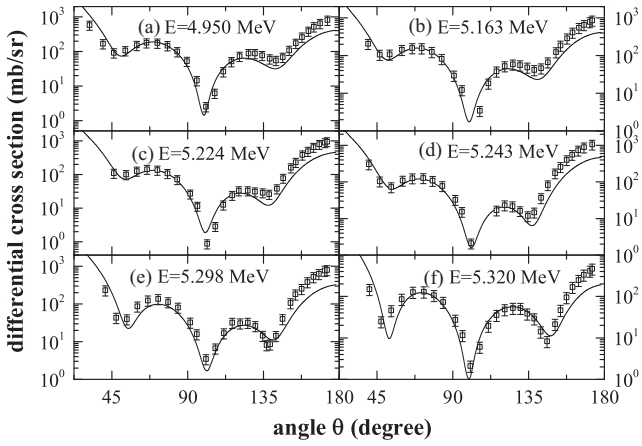

FIG. 37. Fits to the $^{12}C(\alpha,\alpha)^{12}C$ angular distributions of Morris 1968 [35] at (a) $E_{c.m.} = 4.950$, (b) 5.163, (c) 5.224, (d) 5.243, (e) 5.298, and (f) 5.320 MeV.

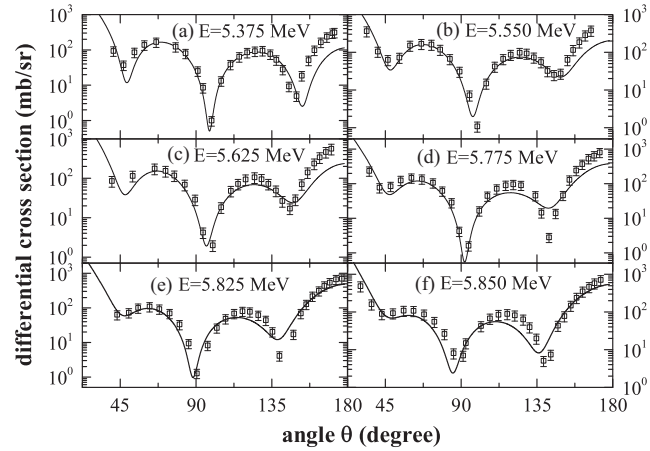

FIG. 38. Fits to the $^{12}C(\alpha,\alpha)^{12}C$ angular distributions of Morris 1968 [35] at (a) $E_{c.m.} = 5.375$, (b) 5.550, (c) 5.625, (d) 5.775, (e) 5.825, and (f) 5.850 MeV.

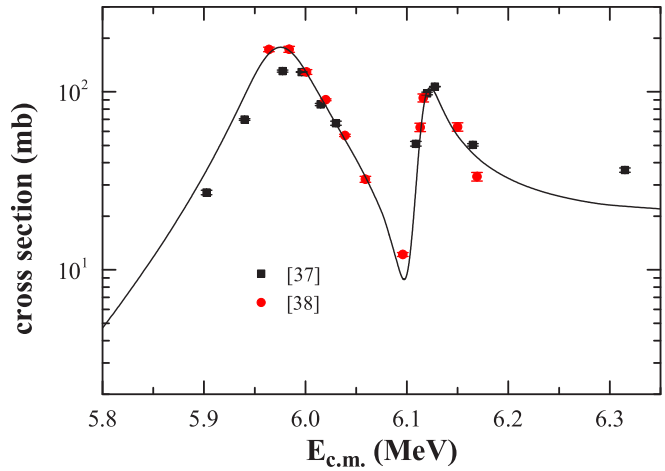

FIG. 39. (Color online) Fits to the $^{12}C(\alpha,\alpha_1)^{12}C$ cross section of Mitchell 1965 [37] and deBoer 2012 [38].

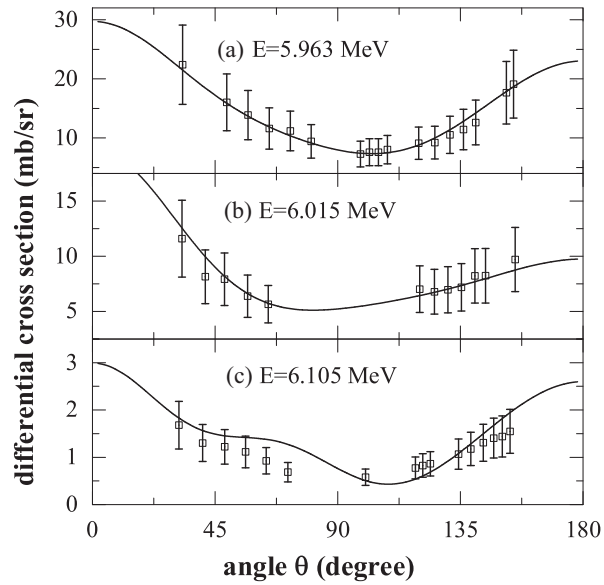

FIG. 40. Fits to the $^{12}C(\alpha,\alpha_1)^{12}C$ angular distributions of Mitchell 1965 [37] at (a) $E_{c.m.} = 5.963$, (b) 6.015, and (c) 6.105 MeV.

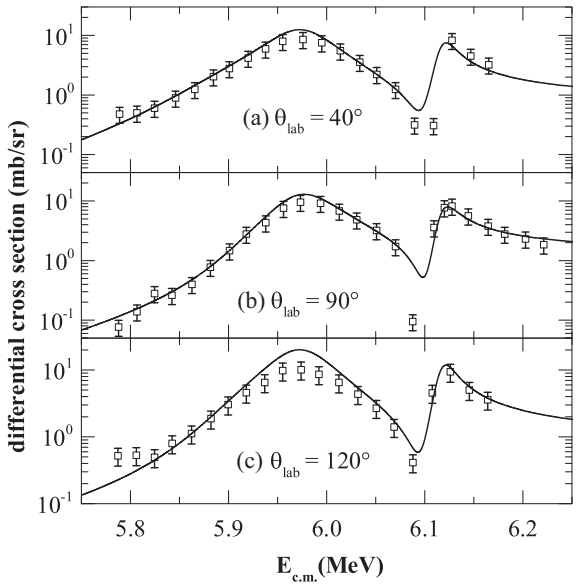

FIG. 41. Fits to the $^{12}C(\alpha,\alpha_1)\,^{12}C$ differential-cross-section data of Mitchell 1965 [37].

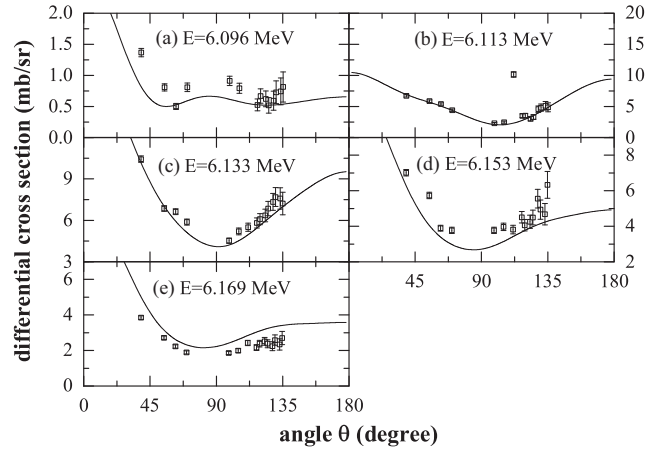

FIG. 43. Fits to the $^{12}C(\alpha,\alpha_1)\,^{12}C$ angular distributions of deBoer 2012 [38] at (a) $E_{c.m.} = 6.096$ MeV, (b) 6.113, (c) 6.133, (d) 6.153, and (e) 6.169 MeV.

number of applications to demonstrate the applicability and versatility of this theory. The final result of $S(0.3\ \text{MeV}) = 162.7 \pm 7.3$ keV b represents the most precise extrapolation of the $^{12}C(\alpha,\gamma)\,^{16}O$ S factor at helium-burning temperatures based on a set of complementary data including all currently available information of ^{16}O system. To the best of our knowledge, this is the first published analysis meeting the precision requirements for $^{12}C(\alpha,\gamma)\,^{16}O$. The whole S factor from 0.3 MeV to 10 MeV provides an astrophysical reaction rate of $^{12}C(\alpha,\gamma)\,^{16}O$ with a sound basis for research into nucleosynthesis and the evolution of stars.

ACKNOWLEDGMENTS

The authors would like to thank Professor Strieder and Dr. deBoer for much help with the data of cascade captures and $^{12}C(\alpha,\alpha_1)\,^{12}C$, respectively. We are also indebted to Professor Brune and Professor Descouvemont for help with their results. In addition, we thank Dr. Tang for reading the manuscript and giving some comments. This work is supported partially by the National Natural Science Foundation of China under Grants No. 11421505, No. 91126017, and No. 11175233, and by the Tsinghua University Initiative Scientific Research Program, China, No. 20111081104.

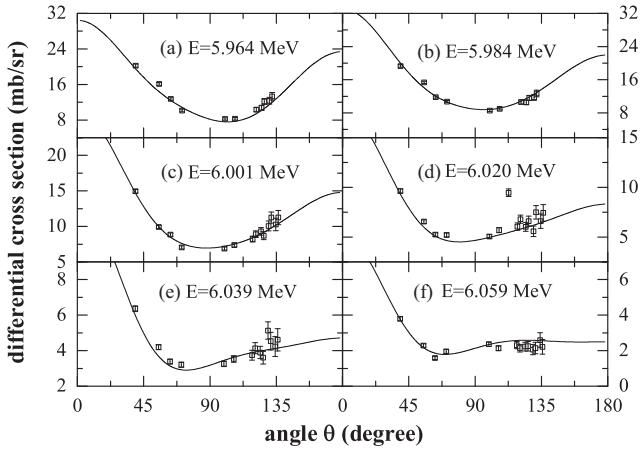

FIG. 42. Fits to the $^{12}C(\alpha,\alpha_1)\,^{12}C$ angular distributions of deBoer 2012 [38] at (a) $E_{c.m.} = 5.964$, (b) 5.984, (c) 6.001, (d) 6.020, (e) 6.039, and (f) 6.059 MeV.

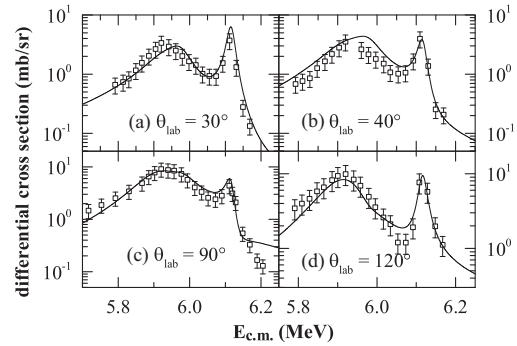

FIG. 44. Fits to the $^{12}C(\alpha,p)\,^{15}N$ differential-cross-section data of Mitchell 1965 [37].

APPENDIX A: DATA SET NORMALIZATIONS

TABLE III. Scaling factors for datasets which have no reported absolute scale, and the normalization coefficient for the absolute data.

Figure No.	Ref.	Normalization	χ^2_C	ndp	Figure No.	Ref.	Normalization	χ^2_C	ndp
4	[7]	$1.03 \times 10^{+00}$	1.437	91	19(b)	[17]	1.29×10^{-08}	3.993	9
4	[8]	$1.03 \times 10^{+00}$	0.959	7	19(c)	[17]	1.08×10^{-08}	1.712	9
4	[10]	$1.00 \times 10^{+00}$	1.056	2	19(d)	[17]	1.25×10^{-08}	1.060	9
4	[9]	$1.03 \times 10^{+00}$	4.196	4	16(a)	[9]	2.21×10^{-10}	2.472	12
5	[26]	$1.00 \times 10^{+00}$	1.406	93	16(b)	[9]	3.13×10^{-10}	2.357	12
5	[27]	$1.00 \times 10^{+00}$	1.406	91	16(c)	[9]	2.20×10^{-09}	0.384	12
5	[28]	$1.00 \times 10^{+00}$	1.406	75	16(d)	[9]	4.33×10^{-10}	1.526	12
27–31	[32]	$1.00 \times 10^{+00}$	1.763	823	Not shown	[9]	1.74×10^{-08}	3.088	12
32–35	[32]	$1.00 \times 10^{+00}$	1.185	794	14(a)	[12]	7.10×10^{-08}	2.800	6
36	[34]	$1.00 \times 10^{+00}$	1.652	128	14(b)	[12]	1.50×10^{-06}	2.806	6
37,38	[35]	$1.00 \times 10^{+00}$	1.034	613	14(c)	[12]	1.18×10^{-05}	2.145	6
Not shown	[36]	$1.00 \times 10^{+00}$	1.060	244	14(d)	[12]	3.04×10^{-07}	1.744	6
6	[12]	$1.00 \times 10^{+00}$	2.690	24	21(a)	[19]	1.93×10^{-06}	3.672	7
6	[8]	$1.03 \times 10^{+00}$	2.327	7	21(b)	[19]	2.21×10^{-06}	1.006	7
6	[13]	9.70×10^{-01}	1.753	9	21(c)	[19]	1.96×10^{-06}	2.862	7
6	[16]	$1.00 \times 10^{+00}$	0.464	20	21(d)	[19]	2.12×10^{-06}	1.536	7
6	[15]	$1.00 \times 10^{+00}$	0.788	20	21(e)	[21]	1.28×10^{-06}	2.867	7
6	[9]	$1.03 \times 10^{+00}$	0.784	4	21(f)	[21]	1.37×10^{-06}	2.415	7
6	[18]	$1.03 \times 10^{+00}$	2.467	4	Not shown	[21]	1.90×10^{-06}	1.264	7
6	[23]	8.70×10^{-01}	1.196	48	21(c)	[20]	$1.10 \times 10^{+00}$	2.980	40
6	[67]	8.00×10^{-01}	1.936	24	22(a)	[19]	2.02×10^{-06}	1.261	4
6	[20]	$1.00 \times 10^{+00}$	0.001	1	22(d)	[19]	1.99×10^{-06}	2.819	20
9–11	[13]	9.70×10^{-01}	1.897	96	22(b)	[21]	1.53×10^{-06}	2.176	13
12	[18]	$1.03 \times 10^{+00}$	2.346	14	22(c)	[21]	1.44×10^{-06}	1.659	13
15(a)	[16]	5.30×10^{-10}	1.675	9	22(d)	[21]	2.12×10^{-06}	1.267	13
15(b)	[16]	4.14×10^{-10}	1.683	9	22(c)	[22]	6.38×10^{-05}	0.785	29
15(c)	[16]	4.68×10^{-09}	1.089	9	22(d)	[22]	1.02×10^{-03}	1.531	14
15(d)	[16]	6.15×10^{-09}	4.002	9	23	[24]	8.00×10^{-01}	2.276	32
15(e)	[16]	5.41×10^{-09}	4.872	9	23	[8]	$1.03 \times 10^{+00}$	0.888	7
15(f)	[16]	1.31×10^{-07}	2.576	9	24	[8]	$1.03 \times 10^{+00}$	1.379	7
20(a)	[14]	2.36×10^{-06}	1.730	9	25	[15]	$1.00 \times 10^{+00}$	1.076	16
20(b)	[14]	2.01×10^{-06}	1.784	9	25	[12]	3.62×10^{-01}	0.745	25
20(c)	[14]	1.48×10^{-06}	1.328	9	25	[23]	3.53×10^{-01}	2.155	21
20(d)	[14]	3.39×10^{-06}	2.857	9	25	[8]	$1.03 \times 10^{+00}$	1.268	7
13(a)	[11]	9.23×10^{-08}	1.884	10	26	[15]	$1.00 \times 10^{+00}$	1.579	16
13(b)	[11]	9.16×10^{-08}	2.213	10	26	[12]	4.42×10^{-01}	2.199	25
13(c)	[11]	8.16×10^{-08}	1.543	10	26	[8]	$1.03 \times 10^{+00}$	0.492	7
13(d)	[11]	6.98×10^{-08}	1.643	10	39	[37]	1.70×10^{-02}	1.560	11
17(a)	[17]	5.08×10^{-10}	4.156	9	39	[38]	$1.00 \times 10^{+00}$	0.380	11
17(b)	[17]	6.49×10^{-10}	2.460	8	40	[37]	$3.66 \times 10^{+00}$	0.037	17
17(c)	[17]	2.01×10^{-09}	2.533	9	40	[37]	$3.60 \times 10^{+00}$	0.068	12
17(d)	[17]	3.42×10^{-09}	0.942	8	40	[37]	1.52×10^{-01}	0.658	16
17(e)	[17]	2.53×10^{-09}	1.599	9	41	[37]	$5.54 \times 10^{+00}$	0.829	21
17(f)	[17]	3.93×10^{-09}	1.708	9	41	[37]	$5.32 \times 10^{+00}$	0.834	25
18(a)	[17]	4.67×10^{-09}	2.490	8	41	[37]	5.58×10^{-01}	1.079	21
18(b)	[17]	5.66×10^{-09}	3.480	9	42	[38]	$1.00 \times 10^{+00}$	2.078	153
18(c)	[17]	1.67×10^{-08}	1.960	9	44	[37]	$4.20 \times 10^{+00}$	0.804	21
18(d)	[17]	3.83×10^{-09}	2.645	9	44	[37]	$2.12 \times 10^{+00}$	0.778	20
18(e)	[17]	9.17×10^{-09}	2.877	9	44	[37]	$1.48 \times 10^{+00}$	0.877	24
18(f)	[17]	1.19×10^{-07}	1.970	9	44	[37]	$1.10 \times 10^{+00}$	0.696	21
19(a)	[17]	2.53×10^{-08}	4.693	9					

APPENDIX B: *R*-MATRIX FIT PARAMETERS

TABLE IV. Parameters obtained from the R-matrix fits, particle partial widths for the levels, and the radiation widths for the γ-ray transitions considered in this work compared with those from the literature.

Res. no.	E_x (MeV)	J_n^π	E_λ (MeV)	$\alpha(I_1+I_2)$	(s,l)	$\gamma_{\alpha sl}$ (MeV)$^{1/2}$	Γ (keV)	Ref. [60]
01	6.049	0_1^+	−0.1113	$\alpha+{}^{12}$C	(0,0)	$-1.37(18)\times10^{-1}$	Fixed	19.7(55)
				$\gamma_0+{}^{16}O_0$	(1,1)	$2.14(41)\times10^{-5}$	$6.88(50)\times10^{-12}$	$6.86(50)\times10^{-12}$
02	12.049	0_2^+	4.865	$\alpha+{}^{12}$C	(0,0)	$4.99(151)\times10^{-3}$	$1.02(25)\times10^{0}$	$1.5(5)\times10^{0}$
				$\gamma_0+{}^{16}O_0$	(1,1)	$6.25(247)\times10^{-4}$		
03	14.032	0_3^+	6.557	$\alpha+{}^{12}$C	(0,0)	$1.65(5)\times10^{-1}$	Fixed	$\Gamma_\alpha/\Gamma_{\rm TOT}=0.9$
04	15.066	0_4^+	7.904	$\alpha+{}^{12}$C	(0,0)	4.33×10^{-1}	Fixed	$\Gamma_\alpha/\Gamma_{\rm TOT}=0.35$
				$\alpha_1+{}^{12}$C	(2,2)	5.91×10^{-2}	Fixed	$\Gamma_{\rm TOT}=166(30)$
				$p+{}^{15}$N	(1,1)	-2.85×10^{-2}	Fixed	
05	BG[a]	0_5^+	30.740	$\alpha+{}^{12}$C	(0,0)	$2.23(9)\times10^{0}$		
				$\gamma_0+{}^{16}O_0$	(1,1)	$-3.01(20)\times10^{-4}$		
06	7.119	1_1^-	−0.4515	$\alpha+{}^{12}$C	(0,1)	-8.08×10^{-2}	Fixed	62.0(170)
				$\gamma_0+{}^{16}O_0$	(1,0)	$2.20(107)\times10^{-4}$	$5.7(3)\times10^{-5}$	$5.5(3)\times10^{-5}$
				$\gamma_0+{}^{16}O_0$	(1,2)	$1.61(46)\times10^{-2}$		
				$\gamma_1+{}^{16}O_1$	(1,0)	$-2.06(898)\times10^{-6}$	$3.0(1)\times10^{-10}$	$<3.0\times10^{-10}$
				$\gamma_2+{}^{16}O_2$	(2,1)	$-7.32(83)\times10^{-4}$	$4.5(1)\times10^{-8}$	$4.6(10)\times10^{-8}$
				$\gamma_3+{}^{16}O_3$	(1,0)	$5.54(1300)\times10^{-6}$	$5.5(2)\times10^{-10}$	$<1.0\times10^{-9}$
				$\gamma_4+{}^{16}O_4$[b]	(0,1)	$-1.00(67)\times10^{-2}$		
07	9.585	1_2^-	2.295	$\alpha+{}^{12}$C	(0,1)	$3.37(3)\times10^{-1}$	322(5)	420(20)
				$\gamma_0+{}^{16}O_0$	(1,0)	$-7.37(25)\times10^{-5}$	$7.25(23)\times10^{-6}$	$1.56(12)\times10^{-5}$
				$\gamma_0+{}^{16}O_0$	(1,2)	$-2.99(9)\times10^{-3}$		
				$\gamma_1+{}^{16}O_1$	(1,0)	$-1.39(15)\times10^{-4}$		
				$\gamma_3+{}^{16}O_3$	(1,0)	$-6.46(45)\times10^{-5}$	$5.8(8)\times10^{-7}$	$1.4(14)\times10^{-6}$
				$\gamma_4+{}^{16}O_4$	(0,1)	$1.36(68)\times10^{-3}$	$1.5(15)\times10^{-6}$	$7.8(16)\times10^{-6}$
08	12.442	1_3^-	5.289	$\alpha+{}^{12}$C	(0,1)	$1.13(2)\times10^{-1}$	162(7)	102(4)
				$\gamma_0+{}^{16}O_0$	(1,0)	$-8.15(137)\times10^{-4}$	$2.3(3)\times10^{-3}$	$1.2(2)\times10^{-2}$
				$\gamma_0+{}^{16}O_0$	(1,2)	$-2.73(13)\times10^{-2}$		
				$\gamma_1+{}^{16}O_1$	(1,0)	$-5.25(59)\times10^{-4}$	$1.2(3)\times10^{-4}$	$1.2(6)\times10^{-4}$
				$\gamma_2+{}^{16}O_2$	(2,1)	$1.39(51)\times10^{-3}$	$3.4(25)\times10^{-5}$	$7.0(30)\times10^{-5}$[c]
				$\gamma_4+{}^{16}O_4$	(0,1)	$2.89(55)\times10^{-3}$	$9.0(34)\times10^{-5}$	$1.3(5)\times10^{-4}$[c]
				$\alpha_1+{}^{12}$C	(2,1)	$1.12(4)\times10^{-1}$	$2.9(2)\times10^{-2}$	2.5×10^{-2}
				$p+{}^{15}$N	(1,0)	$1.16(10)\times10^{-1}$	$1.8(3)\times10^{-1}$	$9.0(1)\times10^{-1}$
09	13.088	1_4^-	5.859	$\alpha+{}^{12}$C	(0,1)	$-4.71(49)\times10^{-2}$	27(4)	45(18)
				$\gamma_0+{}^{16}O_0$	(1,0)	$-3.56(52)\times10^{-3}$	$1.20(4)\times10^{-2}$	$3.2(5)\times10^{-2}$
				$\gamma_0+{}^{16}O_0$	(1,2)	$-2.42(14)\times10^{-2}$		
				$\gamma_1+{}^{16}O_1$	(1,0)	$-7.77(118)\times10^{-4}$	$2.7(8)\times10^{-4}$	$2.4(5)\times10^{-4}$
				$\gamma_2+{}^{16}O_2$	(2,1)	$-3.54(86)\times10^{-3}$	$2.8(13)\times10^{-4}$	$4.0(20)\times10^{-4}$[c]
				$\gamma_4+{}^{16}O_4$	(0,1)	$-9.53(136)\times10^{-3}$	$1.3(4)\times10^{-3}$	$1.35(40)\times10^{-3}$
				$\alpha_1+{}^{12}$C	(2,1)	$8.30(52)\times10^{-2}$	$8.5(9)\times10^{-1}$	1.0×10^{0}
				$p+{}^{15}$N	(1,0)	$2.35(13)\times10^{-1}$	$3.4(4)\times10^{1}$	$1.1(2)\times10^{2}$
10	17.510	1_5^-	9.710	$\alpha+{}^{12}$C	(0,1)	$-8.99(387)\times10^{-2}$	Fixed	29(9)
11	BG	1_6^-	11.434	$\alpha+{}^{12}$C	(0,1)	$1.23(1)\times10^{-2}$		
				$\gamma_0+{}^{16}O_0$	(1,0)	$-5.75(65)\times10^{-4}$		
				$\gamma_0+{}^{16}O_0$	(1,2)	$7.40(237)\times10^{-3}$		
				$\gamma_1+{}^{16}O_1$	(1,0)	$-9.71(133)\times10^{-4}$		
				$p+{}^{15}$N	(1,0)	$-8.95(290)\times10^{-2}$		

TABLE IV. (*Continued.*)

Res. no.	E_x (MeV)	J_n^π	E_λ (MeV)	$\alpha(I_1+I_2)$	(s,l)	$\gamma_{\alpha sl}$ (MeV)$^{1/2}$	Γ (keV)	Ref. [60]
12	6.917	2_1^+	−0.2449	$\alpha+{}^{12}$C	(0,2)	1.68×10^{-1}	Fixed	26.7(103)
				$\gamma_0+{}^{16}O_0$	(1,1)	$1.99(8)\times10^{-3}$	$9.9(3)\times10^{-5}$	$9.7(3)\times10^{-5}$
				$\gamma_0+{}^{16}O_0$	(1,3)	$2.81(37)\times10^{-1}$		
				$\gamma_1+{}^{16}O_1$	(1,1)	$-6.75(5)\times10^{-4}$	$2.7(3)\times10^{-8}$	$2.7(3)\times10^{-8}$
				$\gamma_2+{}^{16}O_2$	(2,0)	$1.30(29)\times10^{-5}$	$9.0(30)\times10^{-9}$	9.0×10^{-9}
				$\gamma_3+{}^{16}O_3$[d]	(1,1)	$1.96(23)\times10^{-2}$		
13	9.844	2_2^+	2.684	$\alpha+{}^{12}$C	(0,2)	$1.34(2)\times10^{-2}$	0.71(19)	0.625(100)
				$\gamma_0+{}^{16}O_0$	(1,1)	$-1.62(3)\times10^{-4}$	$2.0(1)\times10^{-6}$	$5.7(6)\times10^{-6}$
				$\gamma_0+{}^{16}O_0$	(1,3)	$-1.03(3)\times10^{-2}$		
				$\gamma_1+{}^{16}O_1$	(1,1)	$-3.27(43)\times10^{-4}$	$4.4(12)\times10^{-7}$	$1.9(4)\times10^{-6}$
				$\gamma_3+{}^{16}O_3$	(1,1)	$-1.03(9)\times10^{-3}$	$2.1(4)\times10^{-6}$	$2.2(4)\times10^{-6}$
14	11.520	2_3^+	4.314	$\alpha+{}^{12}$C	(0,2)	$6.86(3)\times10^{-2}$	74(1)	71(5)
				$\gamma_0+{}^{16}O_0$	(1,1)	$1.77(17)\times10^{-3}$	$6.8(2)\times10^{-4}$	$6.1(2)\times10^{-4}$
				$\gamma_0+{}^{16}O_0$	(1,3)	$-2.02(15)\times10^{-2}$		
				$\gamma_1+{}^{16}O_1$	(1,1)	$1.64(13)\times10^{-3}$	$3.1(5)\times10^{-5}$	$3.0(5)\times10^{-5}$
				$\gamma_2+{}^{16}O_2$	(2,0)	$2.46(16)\times10^{-4}$	$2.2(3)\times10^{-5}$	2.0×10^{-5}[c]
				$\gamma_3+{}^{16}O_3$	(1,1)	$-1.66(14)\times10^{-3}$	$2.0(3)\times10^{-5}$	$2.9(7)\times10^{-5}$
				$\gamma_4+{}^{16}O_4$	(2,0)	$-1.90(32)\times10^{-4}$	$1.1(4)\times10^{-5}$	$<5.0\times10^{-6}$
15	13.020	2_4^+	5.833	$\alpha+{}^{12}$C	(0,2)	$8.15(20)\times10^{-2}$	112(5)	150(10)
				$\gamma_0+{}^{16}O_0$	(1,1)	$-8.51(66)\times10^{-4}$	$2.2(2)\times10^{-4}$	$7.0(20)\times10^{-4}$
				$\gamma_0+{}^{16}O_0$	(1,3)	$-7.54(74)\times10^{-2}$		
				$\alpha_1+{}^{12}$C	(2,0)	$-4.04(37)\times10^{-2}$	$4.1(8)\times10^{-1}$	$5.0(20)\times10^{-1}$[c]
				$p+{}^{15}$N	(1,1)	$-8.23(45)\times10^{-2}$	$1.6(2)\times10^{0}$	$1.5(2)\times10^{0}$[c]
16	15.90	2_5^+	8.300	$\alpha+{}^{12}$C	(0,2)	$2.22(9)\times10^{-1}$	Fixed	$\Gamma_{\rm TOT}=600$
				$\gamma_0+{}^{16}O_0$	(1,1)	$-1.34(8)\times10^{-3}$	Fixed	$\Gamma_\alpha\Gamma_\gamma/\Gamma_{\rm TOT}=0.4$ eV
17	16.443	2_6^+	9.281	$\alpha+{}^{12}$C	(0,2)	$-3.37(26)\times10^{-2}$	Fixed	$\Gamma_\alpha/\Gamma_{\rm TOT}=0.28$
				$\gamma_0+{}^{16}O_0$	(1,1)	$1.38(7)\times10^{-3}$	Fixed	$\Gamma_\alpha\Gamma_\gamma/\Gamma_{\rm TOT}=0.45$ eV
				$\alpha_1+{}^{12}$C	(2,0)	-9.50×10^{-3}	Fixed	$\Gamma_{\rm TOT}=22(3)$
				$p+{}^{15}$N	(1,1)	8.75×10^{-3}	Fixed	
18	17.129	2_7^+	9.967	$\alpha+{}^{12}$C	(0,2)	-7.68×10^{-2}	Fixed	$\Gamma_\alpha/\Gamma_{\rm TOT}=0.37$
				$\alpha_1+{}^{12}$C	(2,0)	6.62×10^{-3}	Fixed	$\Gamma_{\rm TOT}=107(14)$
				$p+{}^{15}$N	(1,1)	1.88×10^{-2}	Fixed	
19	BG	2_8^+	22.618	$\alpha+{}^{12}$C	(0,2)	$2.22(2)\times10^{0}$		
				$\gamma_0+{}^{16}O_0$	(1,1)	$1.15(14)\times10^{-3}$		
				$\gamma_0+{}^{16}O_0$	(1,3)	$1.67(48)\times10^{-1}$		
				$\gamma_1+{}^{16}O_1$	(1,1)	$1.01(12)\times10^{-2}$		
				$\gamma_3+{}^{16}O_3$	(1,1)	$3.18(21)\times10^{-3}$		
				$\alpha_1+{}^{12}$C	(2,0)	$-4.90(42)\times10^{0}$		
				$p+{}^{15}$N	(1,1)	$-1.35(58)\times10^{0}$		
20	6.1299	3_1^-	−0.1032	$\alpha+{}^{12}$C	(0,3)	$-7.39(17)\times10^{-2}$	5.44(25)	2.35(80)
				$\gamma_0+{}^{16}O_0$	(1,2)	$5.83(31)\times10^{-4}$	$2.47(7)\times10^{-8}$	$2.60(13)\times10^{-8}$
21	11.600	3_2^-	3.969	$\alpha+{}^{12}$C	(0,3)	$3.14(2)\times10^{-1}$	718(10)	800(100)
				$\gamma_2+{}^{16}O_2$	(2,1)	$5.38(3930)\times10^{-5}$	$2.4(346)\times10^{-8}$	1.0×10^{-5}[c]
				$\gamma_3+{}^{16}O_3$	(3,0)	$-1.05(59)\times10^{-4}$	$2.8(31)\times10^{-6}$	1.0×10^{-5}[c]
				$\gamma_4+{}^{16}O_4$	(2,1)	$6.13(540)\times10^{-4}$	$1.6(29)\times10^{-6}$	2.0×10^{-5}[c]
22	13.129	3_3^-	6.082	$\alpha+{}^{12}$C	(0,3)	$1.02(3)\times10^{-1}$	69(5)	90(14)
				$\gamma_0+{}^{16}O_0$	(1,2)	$-1.63(79)\times10^{-3}$	$9.1(30)\times10^{-6}$	1.0×10^{-5}
				$\gamma_2+{}^{16}O_2$	(2,1)	$-1.83(30)\times10^{-2}$	$7.5(25)\times10^{-3}$	8.0×10^{0}[c]
				$\alpha_1+{}^{12}$C	(2,1)	$-2.88(30)\times10^{-1}$	$4.26(32)\times10^{1}$	$2.09(6)\times10^{1}$
				$p+{}^{15}$N	(1,2)	$-1.12(119)\times10^{-3}$	$9.8(6)\times10^{-1}$	1.0×10^{0}

TABLE VI. (*Continued.*)

Res. no.	E_x (MeV)	J_n^π	E_λ (MeV)	$\alpha(I_1+I_2)$	(s,l)	$\gamma_{\alpha sl}$ (MeV)$^{1/2}$	Γ (keV)	Ref. [60]
23	13.259	3_4^-	6.063	$\alpha+^{12}$C	(0,3)	$-3.77(21)\times10^{-2}$	13(4)	9(4)
				$\gamma_2+^{16}O_2$	(2,1)	$-1.79(15)\times10^{-2}$	$8.0(13)\times10^{-3}$	$9.2(15)\times10^{-3}$[c]
				α_1+^{12}C	(2,1)	$3.44(15)\times10^{-2}$	$2.96(36)\times10^{2}$	$8.2(11)\times10^{0}$
				$p+^{15}$N	(1,2)	$4.43(12)\times10^{-1}$	$1.6(1)\times10^{1}$	4.1×10^{0}
24	14.100	3_5^-	7.149	$\alpha+^{12}$C	(0,3)	-5.154×10^{-6}	Fixed	150(75)
				α_1+^{12}C	(2,1)	$-1.03(63)\times10^{-2}$	Fixed	$\Gamma_{\rm TOT}=750(200)$
25	15.408	3_6^-	8.246	$\alpha+^{12}$C	(0,3)	-2.57×10^{-7}	Fixed	$\Gamma_\alpha/\Gamma_{\rm TOT}=0.58$
				α_1+^{12}C	(2,1)	2.24×10^{-1}	Fixed	$\Gamma_{\rm TOT}=133(7)$
				$p+^{15}$N	(1,2)	9.83×10^{-6}		
26	15.828	3_7^-	8.266	$\alpha+^{12}$C	(0,3)	-2.24×10^{-1}	Fixed	$\Gamma_\alpha/\Gamma_{\rm TOT}=0.21$
				α_1+^{12}C	(2,1)	1.03×10^{-2}	Fixed	$\Gamma_{\rm TOT}=703(113)$
27	BG	3_8^-	22.618	$\alpha+^{12}$C	(0,3)	$-1.64(1)\times10^{0}$		
				$\gamma_4+^{16}O_4$	(2,1)	$-1.58(63)\times10^{-2}$		
28	10.361	4_1^+	3.196	$\alpha+^{12}$C	(0,4)	$2.17(3)\times10^{-1}$	28.4(6)	26(3)
				$\gamma_0+^{16}O_0$	(1,3)	$1.15(2650)\times10^{-4}$	$5.6(20)\times10^{-11}$	$5.6(20)\times10^{-11}$
				$\gamma_2+^{16}O_2$	(4,0)	$4.27(47)\times10^{-5}$	$4.7(10)\times10^{-7}$	$<1.0\times10^{-6}$
				$\gamma_3+^{16}O_3$	(3,1)	$-4.25(33)\times10^{-3}$	$5.2(8)\times10^{-5}$	$6.2((6)\times10^{-5}$
29	11.094	4_2^+	3.934	$\alpha+^{12}$C	(0,4)	$9.78(108)\times10^{-3}$	0.296(32)	0.28(5)
				$\gamma_2+^{16}O_2$	(4,0)	$1.05(19)\times10^{-4}$	$3.7(1.3)\times10^{-6}$	$3.1(13)\times10^{-6}$
				$\gamma_3+^{16}O_3$	(3,1)	$7.04(82)\times10^{-4}$	$2.7(6)\times10^{-6}$	$2.5(6)\times10^{-6}$
30	13.879	4_3^+	6.835	$\alpha+^{12}$C	(0,4)	$-5.00(56)\times10^{-2}$	50.3(49)	$\Gamma_\alpha/\Gamma_{\rm TOT}=0.65(5)$
				α_1+^{12}C	(2,1)	$-2.01(14)\times10^{-1}$	$\Gamma_{\rm TOT}=74(7)$	$\Gamma_{\rm TOT}=77(7)$
31	16.844	4_4^+	9.682	$\alpha+^{12}$C	(0,4)	$1.06(21)\times10^{-1}$	Fixed	$\Gamma_{\rm TOT}=567(60),\Gamma_\alpha/\Gamma_{\rm TOT}=0.28$
32	BG	4_5^+	30.230	$\alpha+^{12}$C	(0,4)	$2.10(3)\times10^{0}$		
				$\gamma_3+^{16}O_3$	(3,1)	$-3.44(30)\times10^{-2}$		
				α_1+^{12}C	(2,2)	$-8.50(118)\times10^{-1}$		
33	14.660	5_1^-	7.498	$\alpha+^{12}$C	(0,5)	3.47×10^{-1}	Fixed	$\Gamma_{\rm TOT}=672(11),\Gamma_\alpha/\Gamma_{\rm TOT}=0.94$
34	16.900	5_2^-	9.748	$\alpha+^{12}$C	(0,5)	2.9×10^{-1}	Fixed	$\Gamma_\alpha=700$
35	BG	5_3^-	23.514	$\alpha+^{12}$C	(0,5)	1.21×10^{0}		
36	14.805	6_1^+	7.657	$\alpha+^{12}$C	(0,6)	-2.25×10^{-1}	Fixed	$\Gamma_{\rm TOT}=70(8),\Gamma_\alpha/\Gamma_{\rm TOT}=0.28$
37	16.275	6_2^+	9.133	$\alpha+^{12}$C	(0,6)	2.83×10^{-1}	Fixed	$\Gamma_{\rm TOT}=422(14)$

[a]"BG" is the abbreviation for background level.
[b]Direct capture for $S_{7.12}$.
[c]Reference [53].
[d]Direct capture for $S_{6.92}$.

[1] C. E. Rolfs and W. S. Rodney, in *Cauldrons in the Cosmos* (University of Chicago Press, Chicago, IL, 1988), pp. xi–xii.
[2] H. O. U. Fynbo *et al.*, Nature (London) **433**, 136 (2005).
[3] W. S. E. Woosley and A. Heger, Phys. Rep. **442**, 269 (2007).
[4] S. M. Austin, A. Heger, and C. Tur, Phys. Rev. Lett. **106**, 152501 (2011).
[5] S. M. Austin, C. West, and A. Heger, Phys. Rev. Lett. **112**, 111101 (2014).
[6] C. Tur, A. Heger, and S. M. Austin, Astrophys. J. **718**, 357 (2010).
[7] D. Schürmann *et al.*, Eur. Phys. J. A **26**, 301 (2005).
[8] D. Schürmann *et al.*, Phys. Lett. B **703**, 557 (2011).
[9] R. Plag, R. Reifarth, M. Heil, F. Käppeler, G. Rupp, F. Voss, and K. Wisshak, Phys. Rev. C **86**, 015805 (2012).
[10] K. Fujita *et al.*, Few-Body Syst. **54**, 1603 (2013).
[11] P. Dyer and C. A. Barnes, Nucl. Phys. A **233**, 495 (1974).
[12] A. Redder, H. W. Becker, C. Rolfs, H.-P. Trautvetter, T. R. Donoghue, T. C. Rinckel, J. W. Hammer, and K. Langanke, Nucl. Phys. A **462**, 385 (1987).
[13] J. M. L. Ouellet, M. N. Butler, H. C. Evans, H. W. Lee, J. R. Leslie, J. D. MacArthur, W. McLatchie, H.-B. Mak, P. Skensved, J. L. Whitton, X. Zhao, and T. K. Alexander, Phys. Rev. C **54**, 1982 (1996).
[14] R. Kunz *et al.*, Nucl. Phys. A **621**, 149 (1997).
[15] R. Kunz, M. Jaeger, A. Mayer, J. W. Hammer, G. Staudt, S. Harissopulos, and T. Paradellis, Phys. Rev. Lett. **86**, 3244 (2001).
[16] M. Assunção *et al.*, Phys. Rev. C **73**, 055801 (2006).

[17] M. Fey, Ph.D. thesis, University of Stuttgart, 2004, http://elib.uni-stuttgart.de/opus/volltexte/2004/1683.
[18] H. Makii *et al.*, Phys. Rev. C **80**, 065802 (2009).
[19] J. D. Larson and R. H. Spear, Nucl. Phys. **56**, 497 (1964).
[20] T. R. Ophel, A. D. Frawley, P. B. Treacy, and K. H. Bray, Nucl. Phys. A **273**, 397 (1976).
[21] W. M. G. Kernel and U. von Wimmersperg, Nucl. Phys. A **167**, 352 (1971).
[22] I. V. Mitchell and T. R. Ophel, Nucl. Phys. **58**, 529 (1964).
[23] K. U. Kettner, H. W. Becker, L. Buchmann, J. Görres, H. Kräwinkel, C. Rolfs, P. Schmalbrock, H. P. Trautvetter, and A. Vlieks, Z. Phys. A: At. Nucl. (1975) **308**, 73 (1982).
[24] C. Matei *et al.*, Phys. Rev. Lett. **97**, 242503 (2006).
[25] X. D. Tang *et al.*, Phys. Rev. Lett. **99**, 052502 (2007).
[26] X. D. Tang *et al.*, Phys. Rev. C **81**, 045809 (2010).
[27] R. E. Azuma, L. Buchmann, F. C. Barkeret *et al.*, Phys. Rev. C **50**, 1194 (1994); **56**, 1655 (1997).
[28] Z. Zhao, R. H. France, K. S. Lai, S. L. Rugari, M. Gai, and E. L. Wilds, Phys. Rev. Lett. **70**, 2066 (1993).
[29] C. R. Brune, W. H. Geist, R. W. Kavanagh, and K. D. Veal, Phys. Rev. Lett. **83**, 4025 (1999).
[30] A. Belhout *et al.*, Nucl. Phys. A **793**, 178 (2007).
[31] N. Oulebsir *et al.*, Phys. Rev. C **85**, 035804 (2012).
[32] R. Plaga, H. W. Becker, A. Redder, C. Rolfs, H.-P. Trautvetter, and K. Langanke, Nucl. Phys. A **465**, 291 (1987).
[33] P. Tischhauser, R. E. Azuma, L. Buchmann, R. Detwiler, U. Giesen, J. Görres, M. Heil, J. Hinnefeld, F. Käppeler, J. J. Kolata, H. Schatz, A. Shotter, E. Stech, S. Vouzoukas, and M. Wiescher, Phys. Rev. Lett. **88**, 072501 (2002).
[34] P. Tischhauser *et al.*, Phys. Rev. C **79**, 055803 (2009).
[35] J. M. Morris, G. W. Kerr, and T. R. Ophel, Nucl. Phys. A **112**, 97 (1968).
[36] M. Bruno, I. Massa, A. Uguzzoni, G. Vannini, E. Verondini, and A. Vitale, Nuovo Cimento A **27**, 1 (1975).
[37] I. V. Mitchell and T. R. Ophel, Nucl. Phys. **66**, 553 (1965).
[38] R. J. deBoer *et al.*, Phys. Rev. C **85**, 045804 (2012).
[39] R. J. deBoer *et al.*, Phys. Rev. C **85**, 038801 (2012).
[40] D. Schürmann *et al.*, Phys. Lett. B **711**, 35 (2012).
[41] D. B. Sayre, C. R. Brune, D. E. Carter, D. K. Jacobs, T. N. Massey, and J. E. O'Donnell, Phys. Rev. Lett. **109**, 142501 (2012).
[42] C. Matei, C. R. Brune, and T. N. Massey, Phys. Rev. C **78**, 065801 (2008).
[43] J. W. Hammer *et al.*, Nucl. Phys. A **752**, 514c (2005).
[44] L. Buchmann, R. E. Azuma, C. A. Barnes, J. Humblet, and K. Langanke, Phys. Rev. C **54**, 393 (1996).
[45] M. Gai *et al.* (UConn-Yale-Duke-Weizmann-PTB-UCL Collaboration), J. Phys.: Conf. Ser. **337**, 012054 (2012).
[46] K. E. Rehm, J. Phys.: Conf. Ser. **337**, 012006 (2012).
[47] Y. Xu *et al.*, Nucl. Instrum. Methods Phys. Res., Sect. A **581**, 866 (2007).
[48] A. Lane and R. Thomas, Rev. Mod. Phys. **30**, 257 (1958).
[49] A. Lane and J. Lynn, Nucl. Phys. **17**, 563 (1960).
[50] F. C. Barker and T. Kajino, Aust. J. Phys. **44**, 369 (1991).
[51] R. J. Holt, H. E. Jackson, R. M. Laszewski, J. E. Monahan, and J. R. Specht, Phys. Rev. C **18**, 1962 (1978).
[52] R. E. Azuma *et al.*, Phys. Rev. C **81**, 045805 (2010).
[53] R. J. deBoer, J. Görres, G. Imbriani, P. J. LeBlanc, E. Uberseder, and M. Wiescher, Phys. Rev. C **87**, 015802 (2013).
[54] S. Devons and L. J. B. Goldfarb, in *Handbuch der Physik*, edited by S. Flugge (Springer, Berlin, 1957), Vol. 42, p. 362.
[55] A. J. Ferguson, *Angular Correlation Methods in Gamma-Ray Spectroscopy* (North-Holland, Amsterdam, 1965).
[56] D. L. Smith, *Probability, Statistics, and Data Uncertainties in Nuclear Science and Technology* (American Nuclear Society, Chicago, 1991).
[57] Z. P. Chen, R. Zhang *et al.*, Sci. China, Ser. G: Phys., Mech. Astron. **46**, 225 (2003).
[58] A. D. Carlson, S. A. Badikov, Z. P. Chen *et al.*, Nucl. Data Sheets **109**, 2834 (2008).
[59] A. D. Carlson, V. G. Pronyaev, D. L. Smith, N. M. Larson, Z. P. Chen *et al.*, Nucl. Data Sheets **110**, 3215 (2009).
[60] D. R. Tilley, H. R. Weller, and C. M. Cheves, Nucl. Phys. A **564**, 1 (1993).
[61] E. T. Li, B. Guo, Y. J. Li, Z. H. Li *et al.*, Nucl. Tech. (in Chinese) **37**, 100510 (2014).
[62] X. C. Du, B. Guo, Z. H. Li, D. Y. Pang, E. T. Li, and W. P. Liu, Sci. Chin.-Phys. Mech. Astron. **58**, 062001 (2015).
[63] B. Canbula *et al.*, Nucl. Sci. Tech. **26**, S20504 (2015).
[64] Z. D. Wu, B. Guo, Z. H. Li *et al.*, Nucl. Tech. (in Chinese) **37**, 100512 (2014).
[65] R. Kunz, M. Fey, M. Jaeger, A. Mayer, J. W. Hammer, G. Staudt, S. Harissopulos, and T. Paradellis, Astrophys. J. **567**, 643 (2002).
[66] Y. Xu *et al.*, Nucl. Phys. A **918**, 61 (2013).
[67] F. Brochard, P. Chevallier, D. Disdier, V. Rauch, and F. Scheibling, J. Phys. (Paris) **34**, 363 (1973).
[68] L. Buchmann, G. Ruprecht, and C. Ruiz, Phys. Rev. C **80**, 045803 (2009).
[69] G. Roters, C. Rolfs, F. Strieder, and H. P. Trautvetter, Eur. Phys. J. A **6**, 451 (1999).
[70] L. Gialanella, D. Rogalla, F. Strieder *et al.*, Eur. Phys. J. A **11**, 357 (2001).
[71] M. Dufour and P. Descouvemont, Phys. Rev. C **78**, 015808 (2008).